N U M E R I C A L M O D E L S
OF THE BOUNDARY LAYER

B Y

S V A N T E B O D I N

SVERIGES METEOROLOGISKA OCH HYDROLOGISKA INSTITUT

SWEDEN

1. Background

As we have seen during these days the modelling and simulation of the structure and evolution of the atmospheric boundary layer(ABL) is a formidable task. However, we have also seen great progress in our understanding of primarily turbulence mechanisms in controlling the boundary layer structure. For obvious reasons meteorologists are keen on taking advantage of all these new results and apply them to their forecast problems. My two lectures will deal with the problems involved in trying to formulate more or less operational ABL-models. In some areas very efficient parameterization schemes have been developed while in others we are just at the beginning. As far as I know at the present time no ABL-model is operational. Of course two important problems in this connection are: 1) How do we couple our ABL-model to a large-scale synoptic numerical prediction model? 2) What kind of input data do we need to get reasonably good forecasts over let say 24 h? Most simulations of the ABL have been run from data with fairly high resolution in the vertical. That same resolution is hardly possible in an operational context and analysis and initialization become problems of great importance.
I would like to discuss some of the models that exist today and try to show how they have set out to solve some of the problems involved.
Numerical ABL-models are timeconsuming because of their great complexity. The following list gives a feeling for what the computer-times are for some different kinds of ABL-models.

1. Deardorff's model (1974)	350 h for a 24 h forecast. Δt=6s. 64.000 gridpoints. CDC-7600
2. Pielkes model (1973)	6 h/24h forecast. No physics.CDC-6600
3. White & Tapp (1976)	52 min/24h IBM 360/195 No physics.
4. Long & Shaffer (1975)	10-15m/24h IBM 360/195 "All" physics included.
5. 1-dimensional models	~20s/24h IBM 360/195 physics included.

2,3 and 4 have about the same number of gridpoints, i.e. 8400 (35 x 30 x 8). The one-dimensional models have of the order 30 - 50 gridpoints in the vertical, i.e. more vertical resolution than the 3-dimensional models listed (except Deardorffs). It is obvious that only the last two models meet operational requirements at the present time. The design of efficient finite difference schemes and parameterizations of the physical processes in the ABL is therefore an urgent need in ABL-modelling. It must also be noted that these times do not include initial data processing and analysis.

2. Physical and computational requirements.

What are the physical processes we need to model in a numerical ABL-model? Of course they are not much diffe-

rent from what we need in a large-scale numerical prediction model. However, since the ABL is governed and forced by both the large-scale, non-stationary, synoptic flow as well as being controlled by local processes, e.g. radiation, turbulence, topography, condensation and exchanges through the surface the problem becomes very complicated. The boundary layer depends locally on a number of rather badly known external physical parameters like the type of underlying surface giving variations in albedo, heat capacity and thermal diffusivity in the soil. Soil water content is essential and must be predicted in some way. Figure 1 illustrates this schematically. Many of these processes are neglected in the otherwise sophisticated simulation models of atmospheric turbulence but must be included in an operational model.
How sensitive is a model to different assumptions and parameterizations of various processes and physical characteristics? Some experiments performed with mainly 1-d models give some answers. Of course these are definetly not conclusive.

1. Turbulence is of course what generally defines the boundary layer. All kinds of formulations from simple K-theory to the "higher order closure" schemes are being used today. A constant flux layer for lowest 50 m based on Monin-Obukhov´s similarity theory is often introduced. It seems that most of the problems arise either in very stable conditions when turbulence is weak and patchy or in very unstable conditions. K-theory is based on an assumption of a stationary, horizontally homogenous ABL, conditions which are practically never met in real life. Among the "low-order schemes" it seems that the use of the turbulent energy equation gives the best results with little extra computational time as compared with K-theory (Clarke, Yu (1975)).

2. Radiation is quite important especially, of course, in the nocturnal boundary layer. Fairly fast routines exist today based on emissivity functions for the whole infrared spectral range. When condensation is present (e.g. fog) the radiative properties of fog droplets should be taken into account (Zdunkowski & Barr(1972) and Brown & Roach(1976)).

3. Condensation is also very important for the real life boundary layer. Clouds and fog often form in the ABL changing the properties and structure considerably. Condensation also affects the turbulence. When condensation is present account must also be taken of the settling of fog or cloud drops (Brown & Roach (1976)). The different effects of condensation have not been investigated in the more sophisticated simulation ABL-models.

4. Soil heat and soil water.
This must be included in order to be able to calculate the lower boundary condition for temperature and moisture. The physical constants, thermal conductivity and diffusivity, vary with soil moisture content and from place to place. Initial temperature profiles in the ground are almost never known. Fig. 2 and 3 show the importance of knowing evaporation and soil constants in predicting temperature. The model used is Shaffer & Long´s 1-d model described below.

5. Topography is strongly forcing the ABL. That is also true for variations in roughness, Z_o, as many theoretical and experimental investigations have shown.(And where is the limit between effective Z_o and individual topographic elements?)

6. Most models employ assumptions concerning the surface layer or a K-formulation which are based on a stationary,

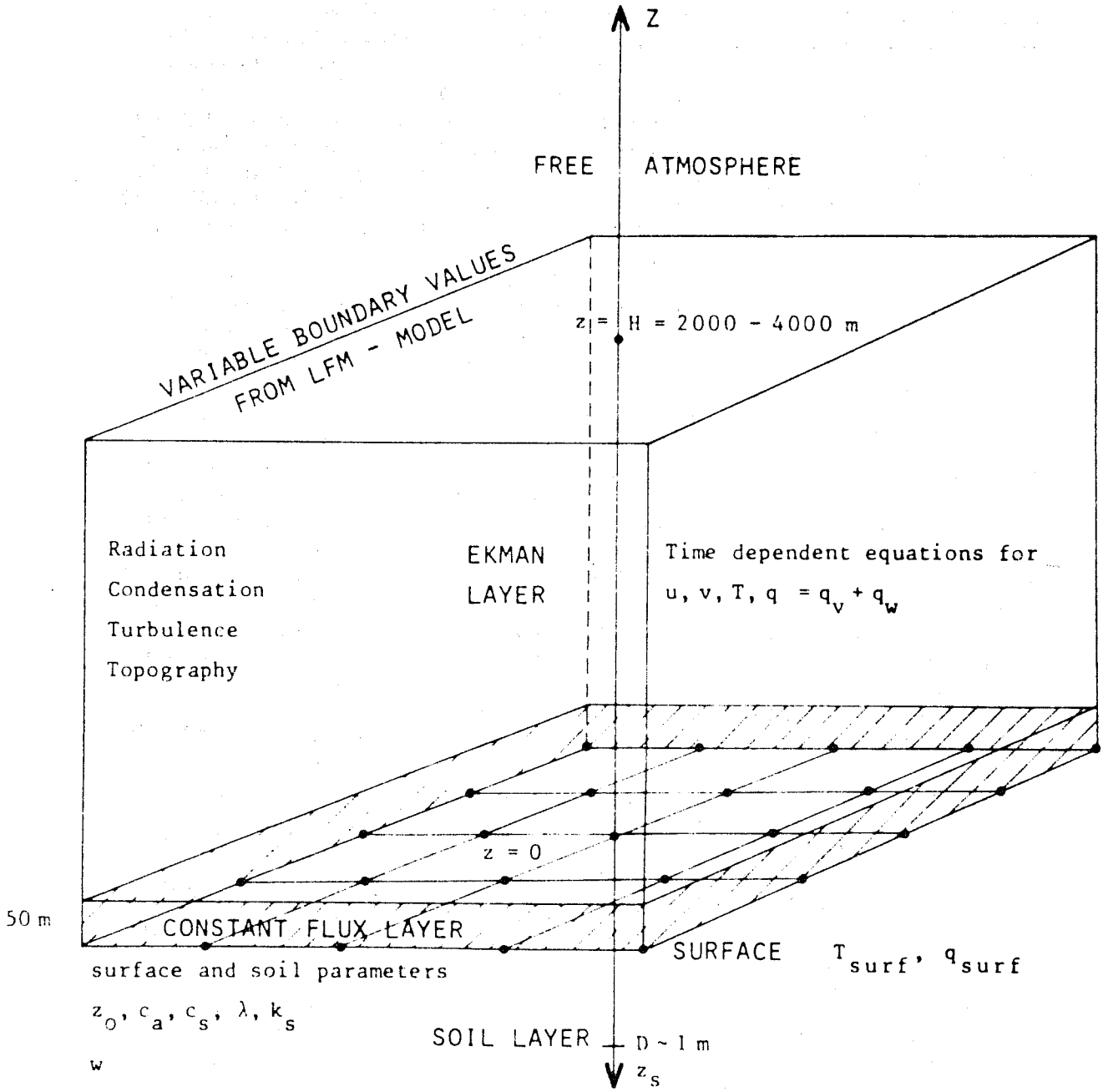

Fig 1 Schematic structure of an Atmospheric Boundary Layer Model. z_0 Roughness parameter, c_a, c_s specific heat for air and soil respectively, λ thermal conductivity and k_s thermal diffusivity in the soil. w is soil water content.

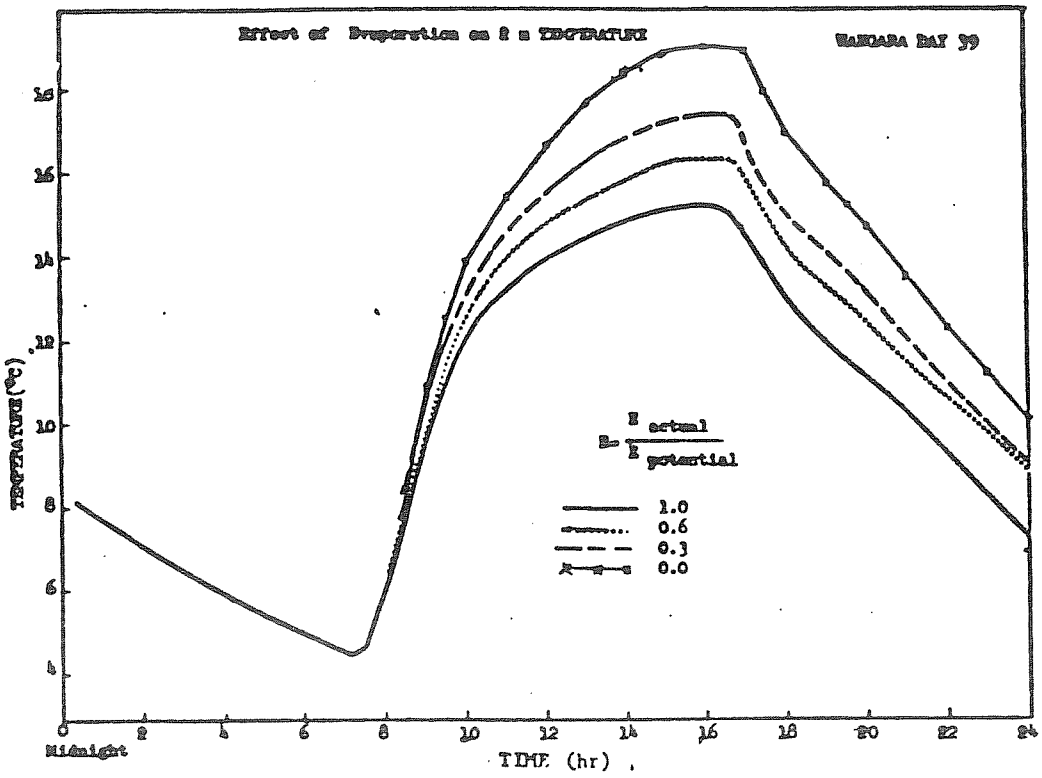

Fig.2 Temperature at 2 m as a function of time for different values of the ratio actual evaporation to potential evaporation, predicted by the one-dimensional version of Shaffer&Long's model. (from Shaffer&Long,1973)

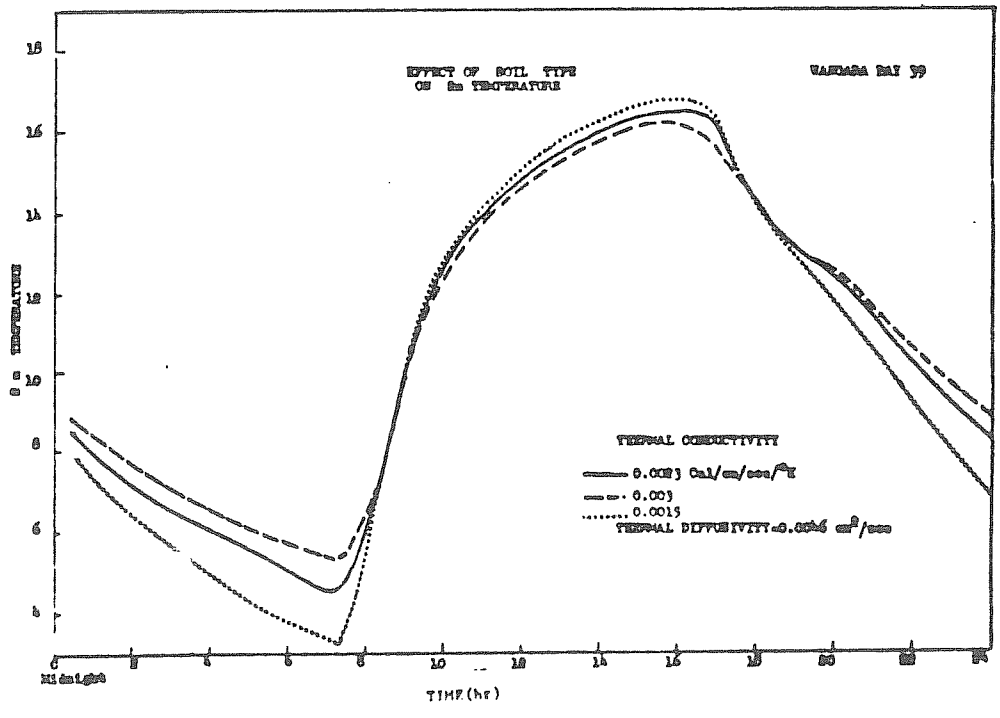

Fig.3 The same as fig.2 but for different values of the thermal conductivity of the soil.

from this ideal state and similarity theory is of little value. The ABL is often baroclinic in contrast to assumed barotropy. Particular to most 1d-models and 3d-models with large horizontal grid distances (~50-100 km) is the introduction of false inertial - diffusive oscillations due to non-stationarity in the geostrophic wind.(Ching & Businger, 1968). They can, however, be eliminated by means of Gutman´s approach also described below. This problem is also clearly associated with the problem of coupling the ABL-model to a limited area fine mesh model (LFM) for the synoptic flow.
Conclusions are that it cannot be stressed enough how important it is for theoretical modelers to treat real boundary layers to a larger extent in order to come up with more efficient parameterizations of the physical processes in the ABL.
There are minimum requirements to the degree of which physical processes should be introduced in ABL-models. The combination of a given computer capacity and numerical efficiency set the limit for the resolution, or griddistance, of a particular model. However, it can be argued that unless you can go down to a horizontal griddistance of the order 10 km it is hardly meaningful to run a 3d-model. Barr & Kreitzberg (1975) argues that in a 3d-model with Δs~100 km each gridpoint will essentially behave as an isolated 1d-model. The only advantage is the recalculation of the synoptic advections with improved accuracy. We can also see this from the following simplified scale analysis.

Gutmans approach and scale analysis of the momentum equation.

Gutman (1969) has suggested a method of treating the equations of motion as applied to meso-scale problems. What he does is to start from the Reynold´s stress equations and split up the mean motion into two components i.e.

$$u = \bar{u} + u', \quad v = \bar{v} + v', \quad w = \bar{w} + w' \qquad (1)$$

This kind of dividing the solution in a linear combination of two or more parts is often done in the solution of partial differential equations.
The advantage is that $\bar{u}$ and u' will satisfy different boundary conditions, thereby simplifying the problem.
We will as an example treat the equation for the u-component of the wind.
The starting equation is

$$\frac{\partial u}{\partial t} + \bar{V} \cdot \nabla_h u + w \frac{\partial u}{\partial z} - f v = -\frac{1}{\rho} \frac{\partial p}{\partial x} + \frac{\partial}{\partial z}\left(K \frac{\partial u}{\partial z}\right) \qquad (2)$$

Here we have only retained the vertical stress component in the form

$$-\overline{u'w'} = K \frac{\partial \bar{u}}{\partial z} \qquad (3)$$

The - and ' notation is admittedly confusing. However, we will assume averaging in the Reynold´s sense only when a bar is applied to a product or second or higher moments. In (1), however the bar and prime only denotes the two parts of the variable. We now want to distinguish between a large scale flow predicted by a LFM and a boundary layer part which will be predicted by our ABL-model. We then define the $\bar{u}$ by

$$\frac{\partial \bar{u}}{\partial t} + \bar{v}\cdot\nabla\bar{u} + \bar{w}\frac{\partial \bar{u}}{\partial z} - f\bar{v} = -\frac{1}{\bar{\rho}}\frac{\partial \bar{p}}{\partial x} + \frac{\partial}{\partial z}\left(\bar{K}\frac{\partial \bar{u}}{\partial z}\right) \qquad (4)$$

where $\bar{K}$ is the exchange coefficient of the large scale model (or an equivalent formulation), i.e. we also set

$$K = \bar{K} + K' \qquad (5a)$$

and in addition

$$p = \bar{p} + p' \qquad p' << \bar{p} \qquad (5b)$$

$$\rho = \bar{\rho} + \rho' \qquad \rho' << \bar{\rho} \qquad (5c)$$

We now introduce (1) and (5) into (2) and subtract eq. (4). We then get formally

$$\frac{\partial u'}{\partial t} + (\bar{v}+v')\nabla u' + v'\nabla\bar{u} + (\bar{w}+w')\frac{\partial u'}{\partial z} + w'\frac{\partial \bar{u}}{\partial z} =$$

$$fv' - \frac{1}{\bar{\rho}}\frac{\partial p'}{\partial x} + \frac{\partial}{\partial z}\left(K'\frac{\partial u}{\partial z}\right) + \frac{\partial}{\partial z}\left(\bar{K}\frac{\partial u'}{\partial z}\right) \qquad (6)$$

Next we define the following scales for the boundary layer varibles (subscript b) and the large scale variables (subscript $_o$).

Variable	BL (primed quantities)	Large-scale flow
w	$w_b \sim 10^{-2}$ m/s	$w_o \sim 10^{-2}$ m/s
u, v	$u_b \sim 10$ -"-	$u_o \sim 10$ -"-
x, y	$L_b \sim 10^4$ m	$L_o \sim 10^6$ m
z	$\zeta_b \sim 10^2$ m	$\zeta_o \sim 10^3 - 10^4$ m
p	$p_b \sim 10^2$ N/m^2	$(\Delta p_o \sim 10^3$ N/m$^2)$
ρ	$\rho_b \sim 10^{-3}$ kg/m^3	$\rho_o \sim 1$ kg/m^3
K	$K_b \sim 10$ m^2/s	$K_o \sim 1$ m^2/s

(K varies, however, considerably in the vertical in the BL itself.)

$$f \sim 10^{-4}\ s^{-1}$$

Now non-dimensionalizing eq. (6) gives

$$\frac{1}{f}\frac{\partial u'}{\partial t} + \frac{u_o}{L_b f}(\bar{v}+v')\nabla u' + \frac{u_o}{fL_o}v'\nabla\bar{u} + \frac{w_o}{\zeta_b f}(\bar{w}+w')\frac{\partial u'}{\partial z} + \frac{w_o}{\zeta_o f}w'\frac{\partial \bar{u}}{\partial z}$$

$$-v' = -\frac{p_b}{\rho_o L_b f u_o}\frac{1}{\bar{\rho}}\frac{\partial p'}{\partial x} + \frac{K_b}{\zeta_b^2 f}\frac{\partial}{\partial z}\left(K'\frac{\partial u}{\partial z}\right) + \frac{K_o}{\zeta_b^2 f}\frac{\partial}{\partial z}\left(\bar{K}\frac{\partial u'}{\partial z}\right) \qquad (7)$$

Here the horizontal and vertical derivatives have been non-dimensionalized with the scales L_b, L_o, ζ_b and ζ_o over which the variables vary with the orders of magnitude given in the table.
We can define the following non-dimensional numbers

1. $Ro_L = \frac{u_o}{fL_o} \sim 10^{-1}$ Large scale Rossby number

2. $Ro_b = \frac{u_0}{f L_b} \sim 10^5 \cdot 10^{-x}$ Boundary layer Rossby number, depending upon the horizontal scale L_b.

3. $Ro_{b,vert} = \frac{w_0}{\zeta_b f} \sim 10^0$ BL, vertical Ro

4. $Ro_{L,vert} = \frac{w_0}{\zeta_0 f} \sim 10^{-1}$ Vertical Ro

5. $P_b/\rho_0 L_b f u_0 \sim 10^5 10^{-x}$ BL pressure term, also depending on L_b.

6. $\frac{K_b}{\zeta_b^2 f} \sim 10^1$ Turbulence in the BL

7. $\frac{K_b}{\zeta_b^2 f} \sim 10^0$ Turbulent interaction between large scale flow and the ABL

8. Coriolis term $\sim 10^0 = 1$

We see that terms 6. and 8. are the largest ones. Not surprising of course. Term 1. and 4. are 2 orders of magnitude less than 6. and can be neglected in the first approximation. 3. is estimated on the assumption that we disregard organized convection. Still 3. and 7. might be important. The two terms 2. and 5. are coupled in magnitudes to the horizontal scale L_b in the boundary layer. Let us now look at this term from the point of view of which smallest scale we actually can resolve in a model instead of the scale expected for typical boundary layer flows.

If the resolvable scale is

$L_b \sim 1000$ km (10^6m) then term 2 & 5 $\sim 10^{-1}$ (griddistance ~300km)

$L_b \sim$ 100 km (10^5) " " " " " $\sim 10^0$ (" " ~ 30km)

$L_b \sim$ 10 km (10^4) " " " " " $\sim 10^1$ (" " ~ 3km)

We see that we have to go down to scales of the order of 10 km to get these terms of equal magnitude as the diffusion term. This is true in the Ekman layer but even more true of course in the surface layer. On the other hand in a 3d-model with $\Delta s \sim 100$ km this term must be at least one order of magnitude less than the diffusion term. This means that such a model probably will react as a series of one-dimensional models. The conclusions can also be formulated: If you can afford a griddistance of 10 km go 3 dimensional, otherwise stay one-dimensional!

<u>One-dimensional models of the "Gutman" kind</u>

Carrying out the approximations based on the scale analysis above in order to get a one-dimensional model gives in its simpliest form

$$\frac{\partial u'}{\partial t} - f v' = \frac{\partial}{\partial z}\left(K' \frac{\partial u}{\partial z}\right) + \frac{\partial}{\partial z}\left(\bar{K} \frac{\partial u'}{\partial z}\right) \qquad (8)$$

Assuming that the large-scale flow is basically nonturbulent and using $u = \bar{u} + u'$ we get

$$\frac{\partial u'}{\partial t} - f v' = \frac{\partial}{\partial z}\left(K' \frac{\partial u'}{\partial z}\right) + \frac{\partial}{\partial z}\left(K' \frac{\partial \bar{u}}{\partial z}\right) \qquad (9)$$

Eq. (9) corresponds to the non-stationary, horizontally homogenous Ekman equations. The thermodynamic equation and a moisture conservation equation can be derived similarely. The v' - equation takes the form

$$\frac{\partial v'}{\partial t} + fu' = \frac{\partial}{\partial z}\left(k'\frac{\partial v'}{\partial z}\right) + \frac{\partial}{\partial z}\left(k'\frac{\partial \bar{v}}{\partial z}\right) \qquad (10)$$

One striking property with (9)-(10) is that from this system we have filtered out the class of inertial-diffusive oscillations mentioned earlier. This is simply because the geostrophic wind is now absent from the equations. This is a very nice advantage of eqs. (9)-(10).

Finite difference schemes.

Most problems in boundary layer meteorology reduce to solving an equation of the type

$$\frac{\partial Q}{\partial t} = \frac{\partial}{\partial z}\left(K\frac{\partial Q}{\partial z}\right) + F \qquad (11)$$

where K is a diffusion coefficient and F represents lower order terms. Long (1975) has given a very good review of more and less wellknown finite difference approximations to (11) in terms of a "computational" diffusion coefficient K_c. This was actually first presented in this room in 1973. In the same paper he also discusses the properties of the finite difference approximations used in Shaffer & Long's model for the horizontal advection terms. Let us study (11) in the form

$$\frac{\partial Q}{\partial t} = K\frac{\partial^2 Q}{\partial z^2} + K'\frac{\partial Q}{\partial z} \qquad (12)$$

where $K' = \frac{\partial K}{\partial z}$ and assume K and K' to be constant.

We define the amplification factor of (12) for a finite difference approximation to be g, if (12) can be written in the form

$$Q_j^{n+1} = g\,Q_j^n \qquad (13)$$

Then the computational diffusion coefficient will be given by

$$e^{-K_c\lambda^2\Delta t} = |g| \qquad (14)$$

or

$$K_c = -\frac{1}{\lambda^2\Delta t}\ln|g| \qquad (15)$$

Two finite difference schemes are of particular interest since they have been widely used in recent years:

1. Dufort-Frankel

$$\frac{Q_j^{n+1} - Q_j^{n-1}}{2\Delta t} = \frac{K}{\Delta z^2}\left(Q_{j-1}^n + Q_{j+1}^n - 2\left(Q_j^{n+1} + Q_j^{n-1}\right)\right) \qquad (16)$$

with $g = \dfrac{2\sigma\cos\lambda\Delta z \pm \sqrt{1-4\sigma^2\sin^2\lambda^2\frac{\Delta z^2}{2}}}{1+2\sigma}$ when K'=0

$\sigma = \dfrac{K\Delta t}{\Delta z^2}$ =Fourier number

if $\sigma > 1/2$ g has an imaginary part and (16) creates a false computational "shear", $\frac{\partial K_c}{\partial z}$.

2. Crank-Nicolson in its generalized form

$$\frac{Q_j^{n+1} - Q_j^n}{\Delta t} = K\left(\mu D^2 Q_j^{n+1} + (1-\mu) D^2 Q_j^n\right) \qquad (17)$$

is stable if $\mu \geq 1/2$

and stable for $\mu < 1/2$ if $\tau \leq \frac{1}{2(1-2\mu)}$

Figure 4. shows the behavior of K_c/K for several different schemes as a function of wave length. σ=0.25 means that the corresponding explicit scheme is stable. Crank-Nicolson and Dufort & Frankel are about the same. Fig. 5 shows the ratio when σ=1.0 and the difference between Dufort-Frankel and Crank-Nicolson becomes more pronounced. σ=1.0 as compared to τ=0.25 means a 4 times longer timestep if K and Δz are constant. Figure 6 finally shows a comparison of RMSE for temperature from a simple integration of the thermal diffusion equation with a diurnally varying lower boundary condition. Level spacing is 50 m and an OBrien K-profile has been used. Timestep is one hour! The comparison is made with a high-resolution run.
The comparison between Crank-Nicolson and Dufort-Frankel shows that Crank-Nicolson is superior when increasing the timestep (i.e. for larger Fourier numbers). The pushing of the weight $\mu \to 1$ prevents almost entirely non-linear instability. For many models the Crank-Nicolson scheme seems to be the natural choice. When μ=1 it is also called Laasonens scheme.

Horizontal finite differences.

In the three-dimensional models also horizontal finite differences must be introduced for the advection terms. No subject has been studied so well as this one in NWP. However, there are other possibilities when coupling advection to implicit methods. The Galerkin approximation method has led to slightly different formulations. An example is the "Chapeau" functions, or functions of local support, suggested by Bradley and discussed in Long & Shaffer (1975).

3. One-dimensional models.

In this section we will discuss the structure of some one-dimensional models. Some results from computations will also be shown. A special role in ABL-modeling has been played by the Wangara-data collected by Clarke et. al. (1971). Since Deardorff's simulation of Day 33 many modelers have used data for that day and Deardorff's results have become more or less a standard to compare with. If you are "better" than Deardorff with less computational time - good. But not all testing of models is done on Day 33. One must also keep in mind that that day has been chosen to eliminate as much as possible the effect of advection. The ABL is dry and no condensation occurs. Hayes is in a very flat area suggesting rather homogeneous conditions. The simulation of Day 33 is a check on the ability of a model to simulate the diurnal course in the ABL, not its general capability in ABL prediction. Of course a basic reguirement on any model is the correct handling of the diurnal cycle under ideal conditions. However, even Day 33 has shown unexpected problems in a badly known geostrophic wind. Temperature advections and large scale vertical motion important for

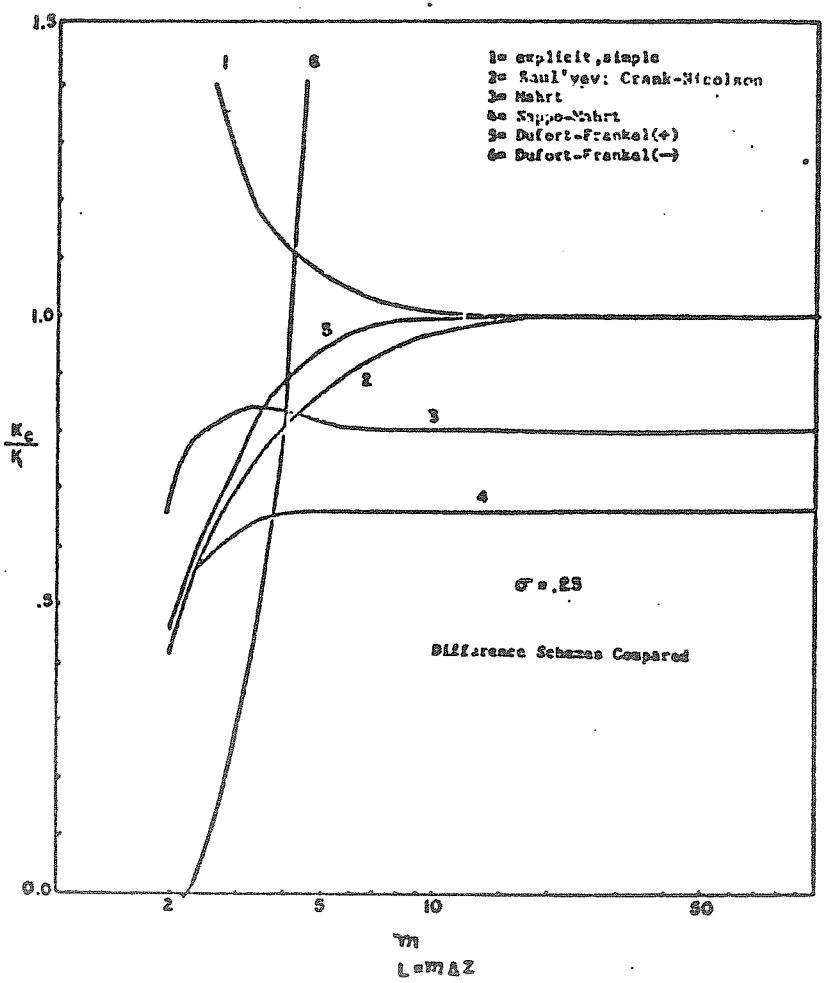

Fig.4 K_c/K for several different finite difference schemes for the diffusion equation. $\sigma = K\Delta t/\Delta z^2 = 0.25$ (from Long, 1975)

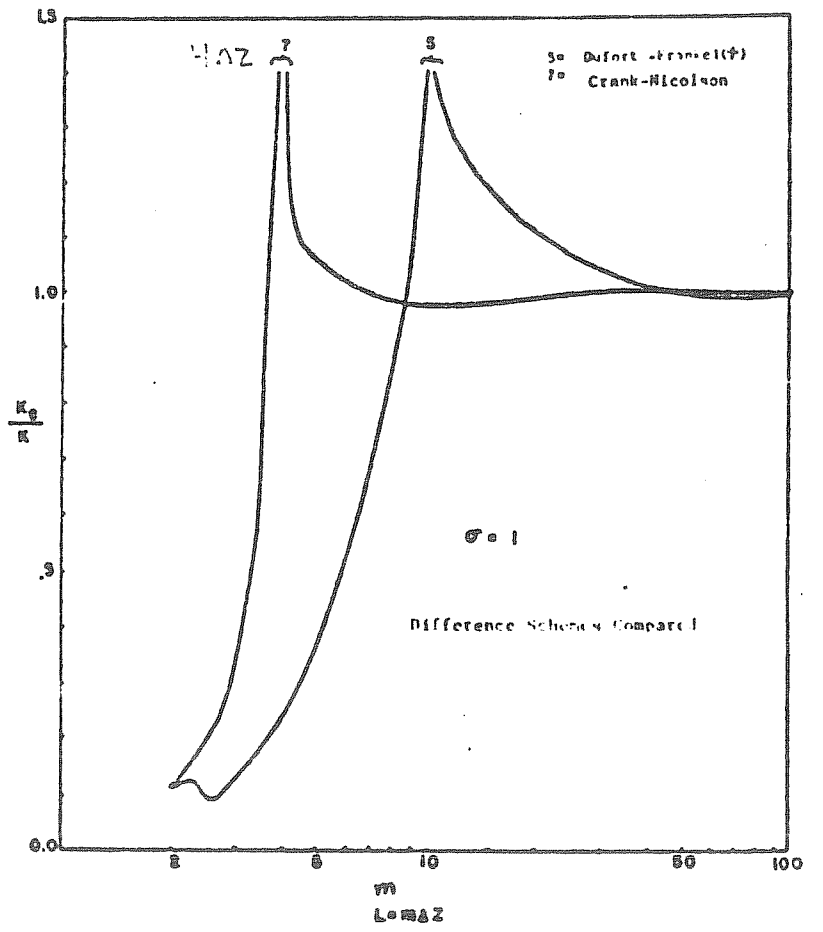

Fig.5 The same as fig.4 but for $\sigma = 1.0$

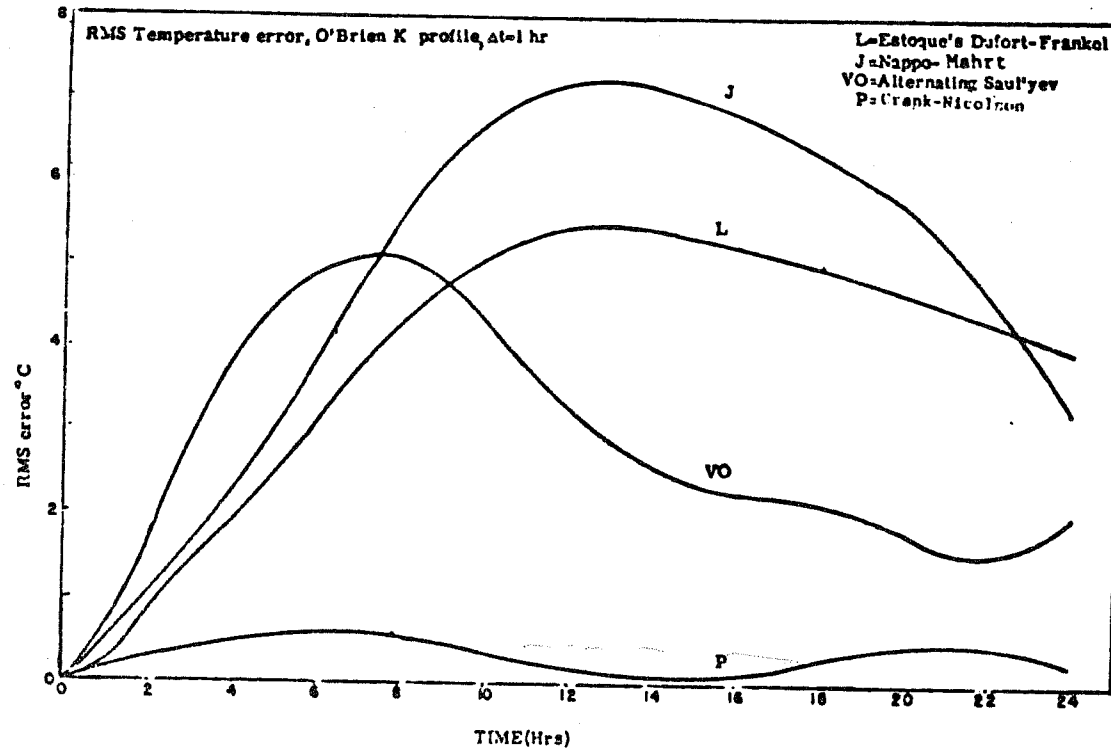

Fig.6 RMS temperature error as a function of time for several diffusion schemes. (Long, 1975)

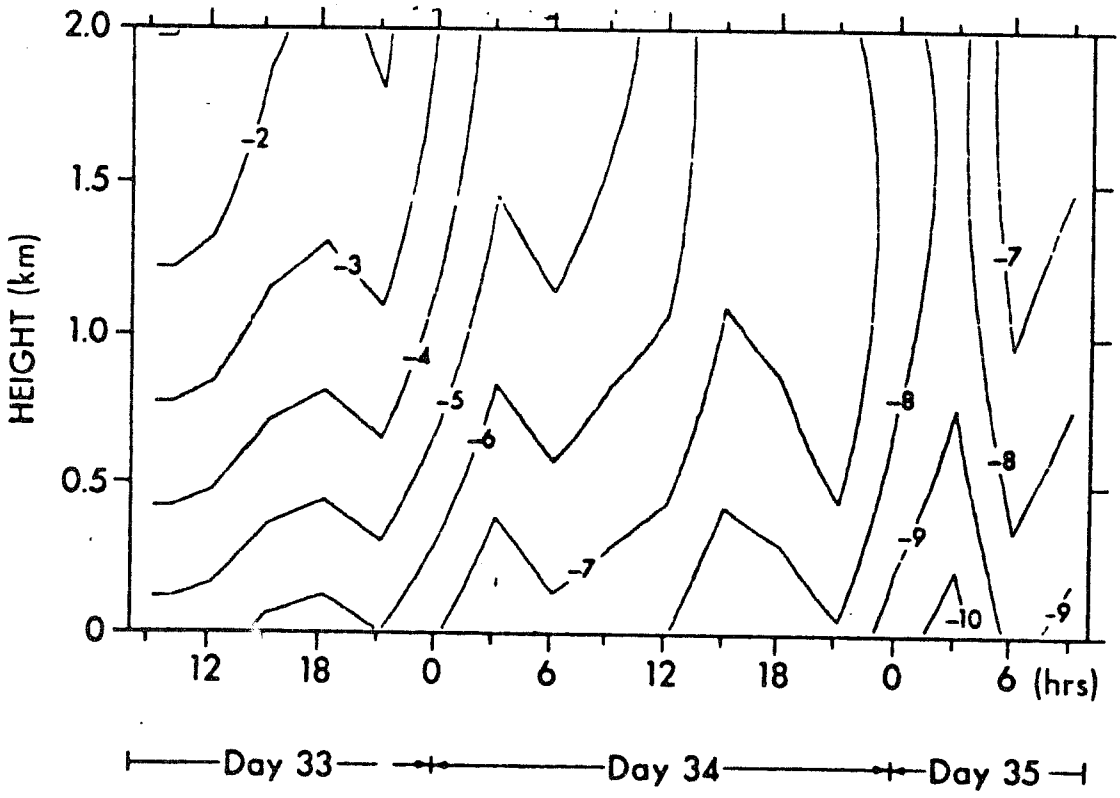

Fig.7 Time-height cross section of the geostrophic wind, u_g, used in Yamada&Mellor's simulation of Day 33-35 of the Wangara data. (from Yamada

the development of the capping inversion of the ABL are present. In the paper by Yamada and Mellor (1975) is presented an extensive simulation of both Day 33 and 34 of the Wangara-data trying to take into account some of these processes. The model is based on a simplification of a "higher order scheme".

a) Yamada & Mellor's model

In this model is used the "level 3 model" for turbulence in the ABL from Mellor and Yamada (1974). The prognostic equations are

$$\frac{\partial u}{\partial t} = fv - f v_g + \frac{\partial}{\partial z}\left(-\overline{u'w'}\right) \tag{18}$$

$$\frac{\partial v}{\partial t} = -fu + f u_g + \frac{\partial}{\partial z}\left(-\overline{v'w'}\right) \tag{19}$$

$$\frac{\partial \theta_v}{\partial t} = \frac{\partial}{\partial z}\left(-\overline{w'\theta_v'}\right) + \frac{T_v}{c}\left(\nu \frac{\partial u_g}{\partial z} - u \frac{\partial v_g}{\partial z}\right) - w\frac{\partial \theta_v}{\partial z} + \sigma_r \tag{20}$$

$$\frac{\partial r}{\partial t} = \frac{\partial}{\partial z}\left(-\overline{w'r'}\right) \tag{21}$$

Here r is mixing ratio, θ_v potential virtual temperature and σ_r the flux divergence of longwave radiation. In the level 3 model for turbulence the turbulent kinetic energy, temperature variance, humidity variance and correlations are forecast by means of

$$\frac{\partial}{\partial t}\left(\frac{q^2}{2}\right) - \frac{\partial}{\partial z}\left(\frac{5}{3}\lambda_1 q \frac{\partial}{\partial z}\left(\frac{q^2}{2}\right)\right) = -\overline{u'w'}\frac{\partial u}{\partial z} - \overline{v'w'}\frac{\partial v}{\partial z} + \beta g \overline{w'\theta_v'} - \frac{q^3}{\Lambda_1} \tag{22}$$

where $q^2/2 = \frac{1}{2}\left(\overline{u'^2} + \overline{v'^2} + \overline{w'^2}\right)$

$$\frac{\partial}{\partial t}\left(\frac{\overline{\theta_v'^2}}{2}\right) - \frac{\partial}{\partial z}\left(\lambda_3 q \frac{\partial}{\partial z}\left(\frac{\overline{\theta_v'^2}}{2}\right)\right) = -\overline{w'\theta_v'}\frac{\partial \theta_v}{\partial z} - q\frac{\overline{\theta_v'^2}}{\Lambda_2} \tag{23}$$

$$\frac{\partial}{\partial t}\left(\frac{\overline{r'^2}}{2}\right) - \frac{\partial}{\partial z}\left(\lambda_3 \frac{\partial}{\partial z}\left(\frac{\overline{r'^2}}{2}\right)\right) = -\overline{w'r'}\frac{\partial r}{\partial z} - q\frac{\overline{r'^2}}{\Lambda_2} \tag{24}$$

primed quantities are turbulent deviations from the mean, unprimed variables. λ_1, λ_3, Λ_1 and Λ_2 are length scales proportional to one length, ℓ, defined by a "Blackadar" relation

$$\ell = \frac{kz}{1 + \frac{kz}{\ell_0}}, \quad \ell_0 = 0.1\,\frac{\int_0^\infty q z\, dz}{\int_0^\infty q\, dz} \tag{25}$$

This seems to be the weakest point in the model. ℓ reaches a maximum value of 80 m where it can be argued that ℓ is of the order 500 m instead in the middle part of the unstable ABL.

From (22)-(24) plus the relation for $(\overline{\theta_v' r'})$ (left out here) one can derive diagnostic relations for the stress tensor and the correlations $\overline{u'\theta_v'}$, $\overline{v'\theta_v'}$, $\overline{w'\theta_v'}$, $\overline{w'r'}$ ..... In Yamada & Mellor's paper they are further simplified to yield relations between an eddy exchange coefficient and $\overline{u'w'}$ etc.

Finite difference approximations

The vertical coordinate z is transformed to a new one by means of

$$\zeta = a_1 z + a_2 z^2/a_3 \tag{26}$$

This is frequently done nowadays. 80 equidistant points in ξ are used between the ground and 2000 m. The time integration is done by means of Laasonen's scheme described above. Δt is 60 s.

Boundary conditions and initial data

This model does not use an independent surface temperature calculation but instead uses the Screen level (1.2m) temperature as a lower boundary condition. A logarithmic profile is used for the lower boundary condition for the wind. At z=2000 m $q^2=\overline{\theta_v'^2}=0$ and

$$\frac{\partial u}{\partial z}=\frac{\partial v}{\partial z}=0 \qquad \frac{\partial \theta_v}{\partial z}=0.001\ K\,m^{-1}$$

Initial data are taken from Day 33 at 0900 LT.

Variation of geostrophic wind and vertical velocity

Y & M have taken a lot of pain in deducing vertical profiles of the geostrophic wind and vertical velocity, and their variation in time.

This is important since the wind profiles are sensitive to the specification of $\mathbf{V}_g$ in Ekman type models of this kind. The geostrophic wind, however, is badly known and the wind at 2000 m is far from the derived geostrophic one. The same is also true for w. Fig. 7 and 8 show the derived time-cross sections of U_g and W. Fig. 9 through 11 show the results of the 48-h integration of T,θ and the u-component of the wind. The diurnal cycle in T is well depicted. However, the night inversion is too low. The daytime θ_v-profiles show good agreement with the observed ones. However, the inversion height seems to be too low in this case too, e.g. 12 o'clock. The wind is realistically predicted and partly the strong forcing by the geostrophic wind causes a nocturnal jet to form around 0130. Fig. 12 shows the evolution of boundary layer height. It is slightly too low during the day. The upper inversion is strongly affected by the imposed large scale vertical velocities when turbulence is absent.

This very complete simulation raises many questions concerning data requirements for ABL-models. In this simulation we already know the result of the surface energy balance by means of the screen level temperature. The results are sensitive to two badly known variables V_g and W. The nocturnal jet can be moved around practically at free will by changing the variation of the geostrophic wind as pointed out by Paul Long.

Gutman's model

In Speranskiy, Lykosov and Gutman (1975) is reported a simulation of O'Neill data by the latest version of Gutman's model, which is supposed to be going to be used operationally in Novosibirsk in the USSR.

The model equations are derived in the way described earlier with some modifications to include effects of a sloping underlying surface and effects of advection of large scale properties by the boundary layer wind, $\mathbf{V}'$.

$$\frac{\partial u'}{\partial t}=\frac{\partial}{\partial z}\left(K\frac{\partial u'}{\partial z}\right)+fv'+\frac{\partial \delta}{\partial x}\left(\frac{g}{\theta}\theta'+0.61q'\right) \qquad (27)$$

$$\frac{\partial v'}{\partial t}=\frac{\partial}{\partial z}\left(K\frac{\partial v'}{\partial z}\right)-fu'+\frac{\partial \delta}{\partial y}\left(\frac{g}{\theta}\theta'+0.61q'\right) \qquad (28)$$

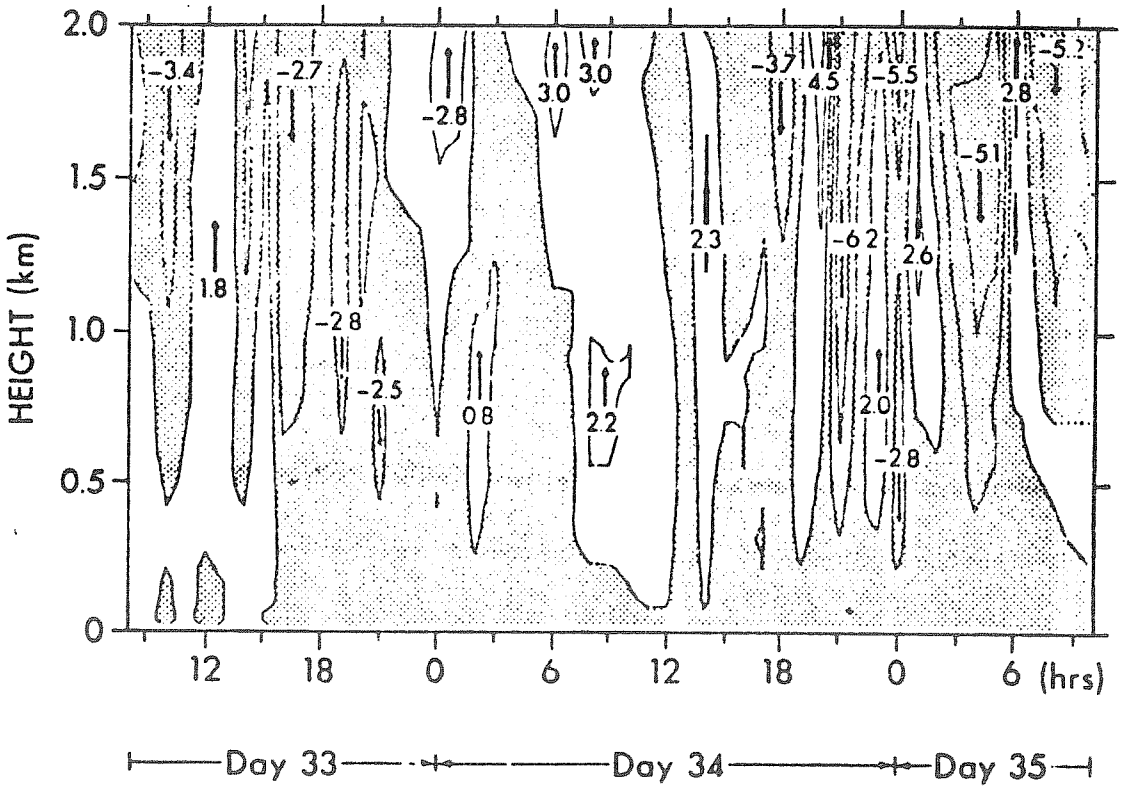

Fig.8 The same but for vertical velocity w in cm/s.

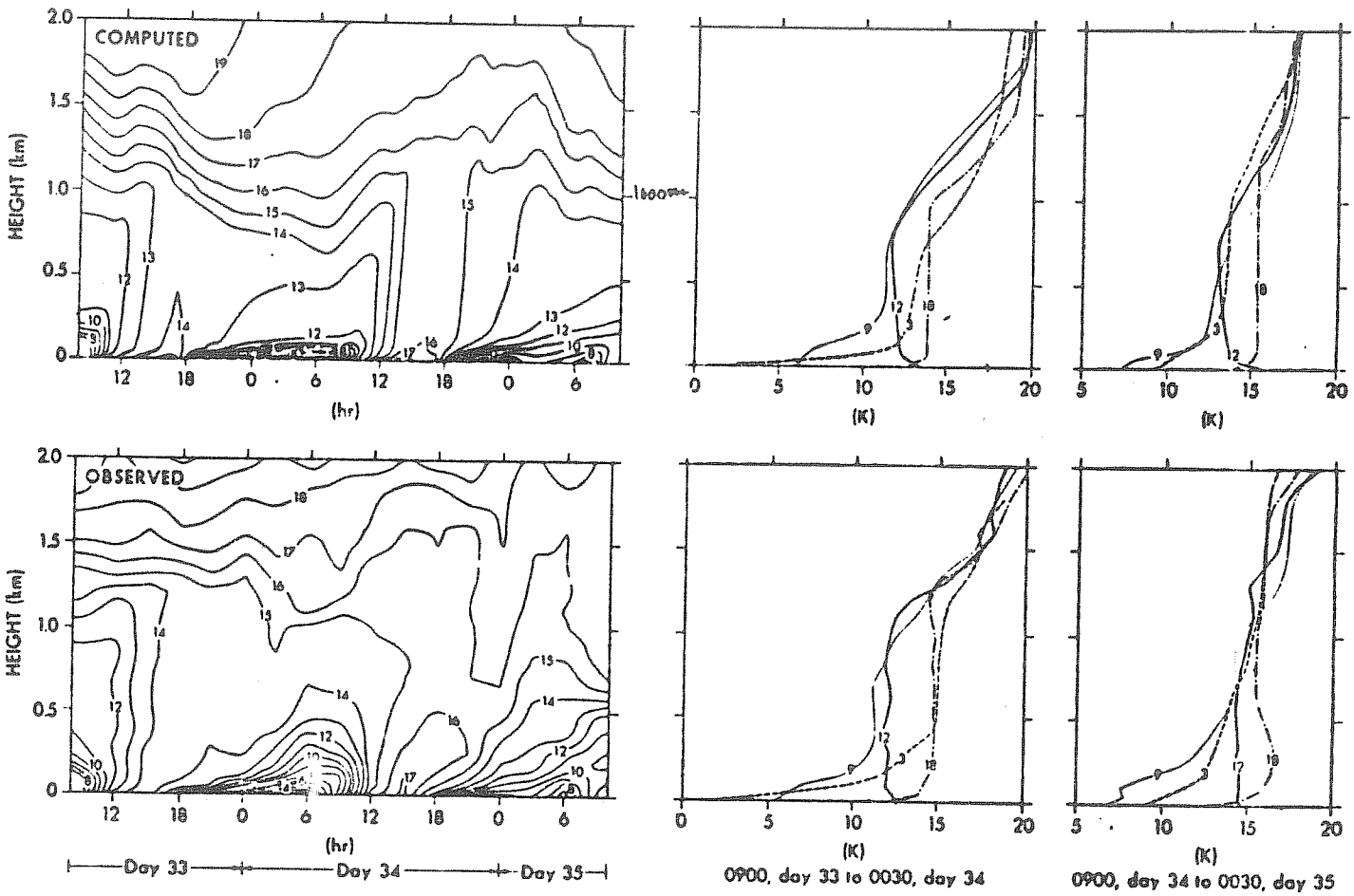

Fig.9

Fig.10

Computed and observed virtual potential temperature (Yamada&Mellor,1975)

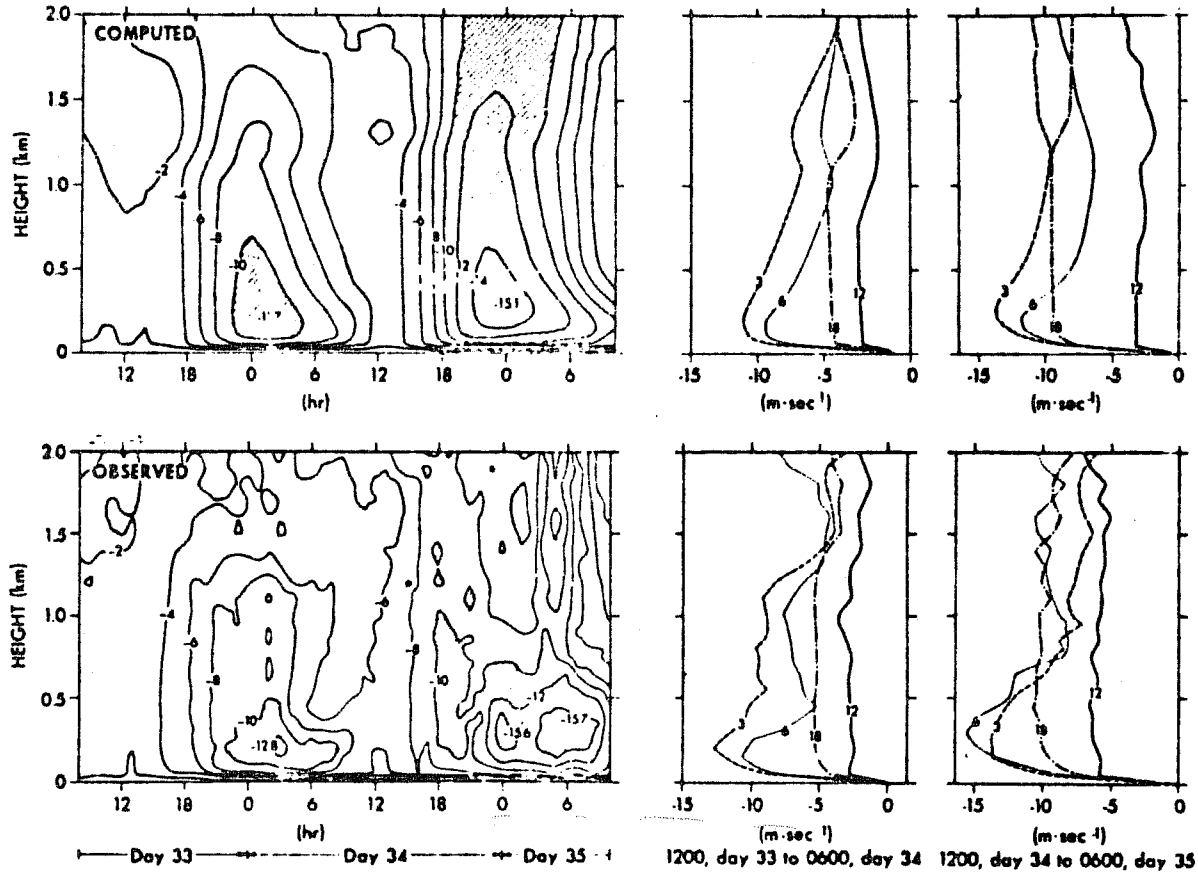

Fig.11 The computed and observed u-component of the wind

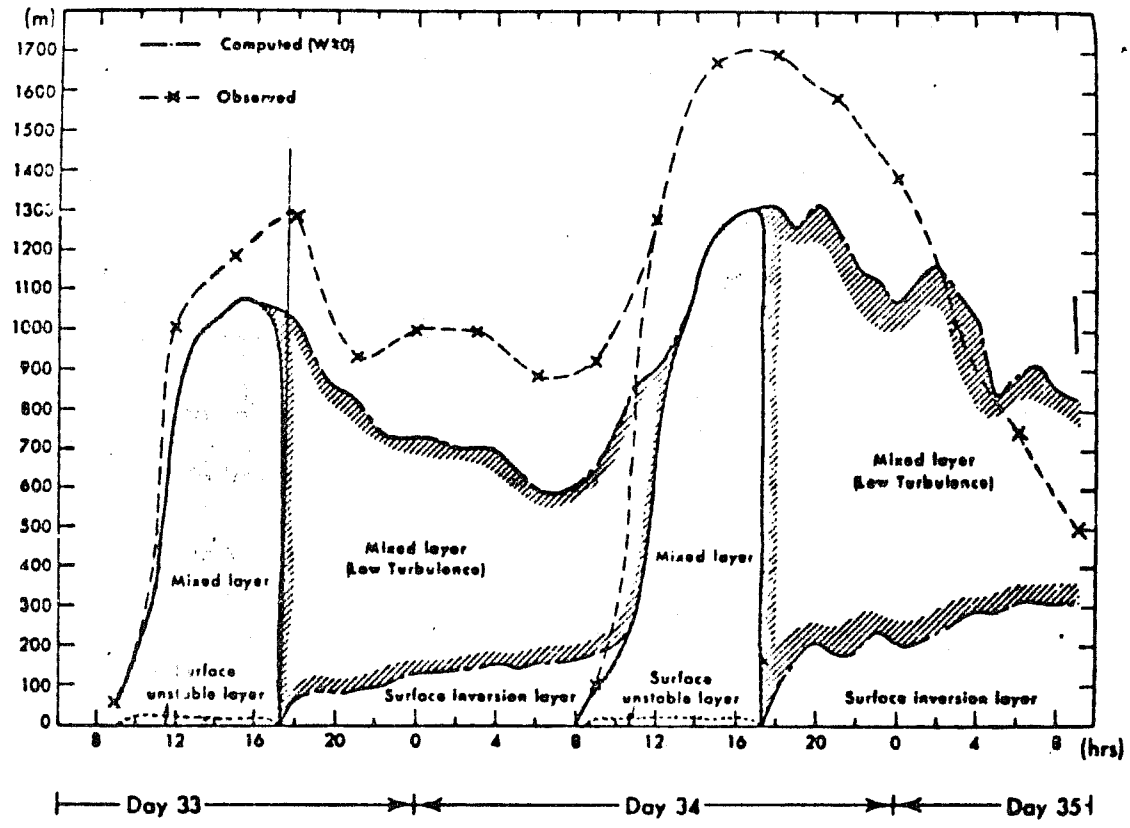

Fig.12 The computed and observed evolution of the boundary layer structure (Yamada&Mellor,1975)

$$\frac{\partial \theta'}{\partial t} = \frac{\partial}{\partial z}\left(K\frac{\partial \theta'}{\partial z}\right) - u'\left(\frac{\partial \bar{\theta}}{\partial x} + \frac{\partial \bar{\theta}}{\partial z}\frac{\partial \delta}{\partial x}\right) - v'\left(\frac{\partial \bar{\theta}}{\partial y} + \frac{\partial \bar{\theta}}{\partial z}\frac{\partial \delta}{\partial y}\right) \qquad (29)$$

$$\frac{\partial q'}{\partial t} = \frac{\partial}{\partial z}\left(K\frac{\partial q'}{\partial z}\right) - u'\left(\frac{\partial \bar{q}}{\partial x} + \frac{\partial \bar{q}}{\partial z}\frac{\partial \delta}{\partial x}\right) - v'\left(\frac{\partial \bar{q}}{\partial y} + \frac{\partial \bar{q}}{\partial z}\frac{\partial \delta}{\partial y}\right) \qquad (30)$$

$$\frac{\partial b}{\partial t} = a_b\frac{\partial}{\partial z}\left(K\frac{\partial b}{\partial z}\right) - \frac{a_d b^2}{K} - \overline{u'w'}\frac{\partial u}{\partial z} - \overline{v'w'}\frac{\partial v}{\partial z} - \frac{g}{\theta}\overline{\theta' w'} \qquad (31)$$

where b is the turbulent energy, $b=\frac{1}{2}(\overline{u'^2}+\overline{v'^2}+\overline{w'^2})$, $a_b=0.073$ and $a_d=0.046$. The notation is the same as above. θ is potential temperature. δ is a function of x and y, $\delta(x,y)$, describing the topography suitably smoothed. The vertical coordinate z_1 is transformed according to $z=z_1-\delta(x,y)$
The underlined terms depend on background variables and must be given.
For turbulence closure the following assumptions are made

$$K = k\left[\int_{z_0}^{z}\frac{dz}{\sqrt{b}} + \frac{z_0}{\sqrt{b_0}}\right] \qquad (32)$$

where k is Von Karmans constant.

$$\frac{g}{\theta}\overline{\theta' w'} = \frac{g}{\theta}K\frac{\partial \theta}{\partial z} + 0.61 g K\frac{\partial q}{\partial z} \qquad (33)$$

$$\overline{u'w'} = -K\frac{\partial u}{\partial z} \qquad \overline{v'w'} = -K\frac{\partial v}{\partial z} \qquad (34)$$

Boundary conditions

at $z=0$: $u'=-\bar{u}$ $v'=-\bar{v}$ $K\frac{\partial b}{\partial z}=0$

$q=\eta q_s$ where η is a specified relative humidity.

A surface energy balance is used to calculate the surface temperature based on a simplified treatment of incoming and outgoing radiation at the surface (Albrecht's and Brunt's relations). No radiation in the ABL is present.

$$Z = H: \quad u' = v' = \theta' = q' = b = 0$$

In order to calculate the energy balance the heat flux from the ground is needed. Soil temperature is predicted by

$$\frac{\partial T_s}{\partial t} = K_s\frac{\partial^2 T_s}{\partial z^2} \qquad (35)$$

where K_s is thermal diffusivity.
Eq.(32) can be written

$$K = l\,b^{1/2} \qquad (36)$$

if

$$l = \frac{k}{b^{1/2}}\left(\int_{z_0}^{z}\frac{dz}{\sqrt{b}} + \frac{z_0}{\sqrt{b_0}}\right) \qquad (37)$$

where (36) is the usual closure assumption. This specification of ℓ is probably the weakest point of the model because (37) relates turbulence at one level to what has happened below, which is not the case in, for example, stable conditions.

Simulation of O´Neill data 24-25 August 1953.

Without going into all the details of specifying the constants, parameters and initial data we will present results from a 48 h simulation starting 1200 LT 24 August. Only the second day is shown below. Gutman reports on 4 experiments where gradually topography and heat advection are taken into account. Advective effects seem to be of the greatest importance. Figure 13 shows observed and predicted temperatures (a,b) and wind velocity (c,d). On the whole this is a fairly good simulation even if the pictures are rather small and difficult to compare. The effect of permitting the background wind to vary in time and possessing a vertical shear is also evident from the other reported experiments in this paper.

Bodin´s model

Bodin (1976) uses a flat surface in (27) and (28). However, the thermodynamic equation looks different because of the inclusion of condensation processes. In this case it is derived from the conservation of static energy and takes on the form

$$\frac{\partial T'}{\partial t}+\bar{w}\left(\frac{\partial T'}{\partial z}+\Gamma_d\right)=\frac{\partial}{\partial z}\left(K_H\left(\frac{\partial T}{\partial z}+\Gamma_d+\frac{L}{c_p}\frac{\partial q_s}{\partial z}-\gamma_{cg}\right)\right)-\frac{L}{c_p}\frac{dq_s}{dt}+\frac{1}{c_p}\frac{\delta Q'}{\delta t} \qquad (38)$$

where γ_{cg} is a counter gradient heat flux correction given by Deardorff (1973)

$$\gamma_{cg}=1\alpha\overline{(w'\theta')}_s \Big/ \left(\frac{1}{\theta}\left(\overline{w'\theta'}\right)_s h\right)^{1/3} h \qquad (39)$$

$\overline{(w'\theta')}_s$ is the surface heat flux and h the height of the ABL.

If $\overline{(w'\theta')}_s \leq 0 \quad \gamma_{cg}=0$

Moisture is predicted by

$$\frac{\partial q}{\partial t}+\bar{w}\frac{\partial q'}{\partial z}=\frac{\partial}{\partial z}\left(K_q\frac{\partial q}{\partial z}\right)+SS \qquad (40)$$

and turbulent energy by

$$\frac{\partial b}{\partial t}=K\left(S^2-a_T\frac{g}{\theta}\left(\frac{\partial\theta}{\partial z}+\frac{L}{c_p}\frac{\partial q_s}{\partial z}-\gamma_{cg}\right)\right)+a_b\frac{\partial}{\partial z}\left(K\frac{\partial b}{\partial z}\right)- \qquad (41)$$

$$-\frac{(0.2b)^{3/2}}{\ell}$$

$$K=\ell(0.2b)^{1/2} \qquad a_T=1.35 \quad a_b=1.2$$

The boundary conditions are similar to Gutman´s.

For the mixing length Deardorff has suggested the following form for ℓ in unstable conditions, $\overline{(w'\theta')}_s>0$:

$$\frac{1}{\ell}=\frac{1}{\ell_N}-\frac{1}{h}\,\frac{\left(1+1.32\frac{z+z_0}{h}\right)}{\left(0.00+\frac{k(z+z_0)}{h}\right)}\cdot\frac{1}{1-50\left(\frac{L_0}{h}\right)} \qquad (42)$$

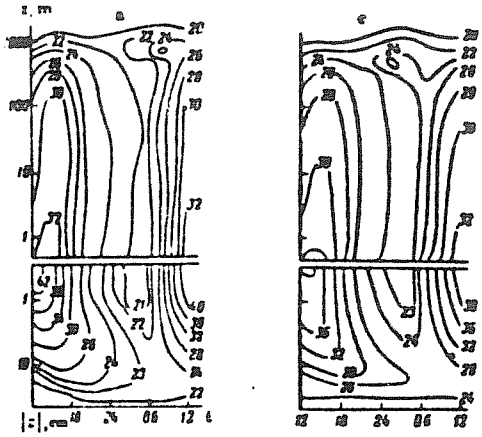

Fig.13

Observed and predicted (left to right) temperature and windspeed time-height cross sections from the O´Neill data,24 August,1200 hours through 25 August,1200 hours. (from Speranskiy,Lykosov and Gutman,1975)

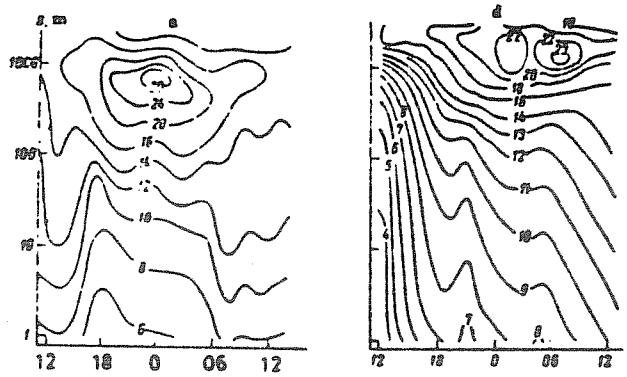

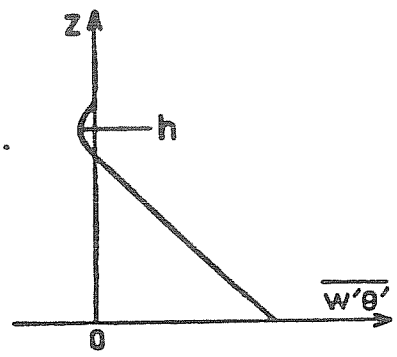

Fig.14 a) Determination of boundary layer height in Bodin´s model from the heat flux profile.

Fig.14 b) Predicted heat flux profiles for Day 33 of the Wangara data with Bodin´s model.

where $\frac{1}{\ell_N} = \frac{1}{k(z+z_0)} + \frac{1}{0.2h}$ (43)

and where h is the height of the ABL determined as shown in fig. 14 where also the form of ℓ is shown. When $(\overline{w'\theta'})_s \leq 0$ h is taken as $0.06 \cdot u_*/|f|$ and

$\ell = \ell_N$ from (43).

This gives a smooth interpolation of ℓ through $L_o \to \infty$; where L_o is the surface Monin-Obukov length.

Numerical solution

A new coordinate ξ is introduced by means of

$$\xi = A_1 \ln \frac{z+z_0}{z_0} + A_2 z + A_3 \quad (44)$$

where A_1, A_2 and A_3 are suitably chosen constants. Laasonens scheme is used in time and centered second order finite differences in the vertical coordinate ζ. In the simulations 35 points have been used between the surface and 2000 m. The timestep has been 2 minutes. The vertical grid is staggered.

The surface temperature is going to be calculated from a prognostic equation.

$$C_* \frac{\partial T}{\partial t} = \left(\rho c_p K_H \left(\frac{\partial \theta}{\partial z} - \gamma_{cg}\right) + \rho L K_q \frac{\partial q}{\partial z} + \lambda \frac{\partial T_{soil}}{\partial z} - F_{long} + F_{sun}\right)_{z=0} \quad (45)$$

where C_* is a mean value of the specific heat in the ground and the air.

For the soil temperature eq. (35) is solved. The lower boundary condition for humidity q(z=0) will be computed from the ratio of actual evaporation to potential evaporation

$$E/Ep = f(w) \quad (46)$$

where f(w) is a function of soil water content, calculated with a special soil water model.

The present model has been used to simulate Day 33 of the Wangara data with a prescribed surface temperature and no radiative flux divergence. The background variables have been varied in time but without vertical shears. Figure 15 shows the evolution of the boundary layer height, h, predicted by the model starting from initial data at 0900 LT. Fig. 16 shows vertical temperature profiles during the day and the night with verification. The daytime profiles seems to be about one degree to cold while the nocturnal profiles are very good except above the mixed layer where radiative and advective effects are strong. Fig. 17 shows the predicted u-component of the wind (compare fig. 11). A nocturnal jet develops, but about 2 1/2 h later than observed. However, in this simulation no shear in the background wind is present. The model is now being tested with a complete radiation calculation and surface energy treatment. The different formulation of ℓ and the use of the turbulent energy equation allow the unstable boundary layer to grow in a realistic way.

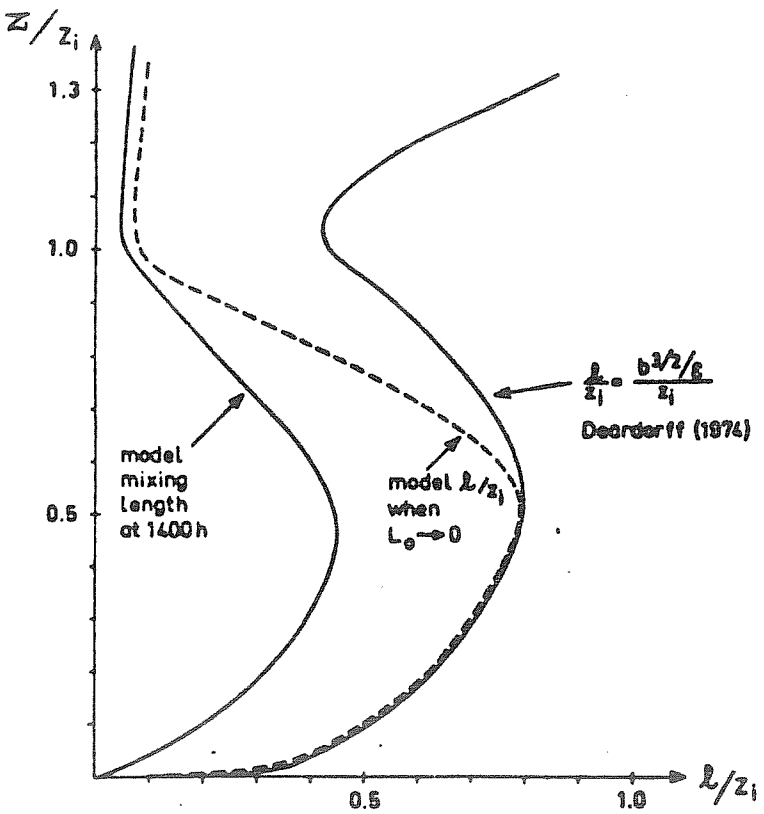

Fig.14 c) Mixing length used for unstable conditions in Bodin´s model as suggested by Deardorff.

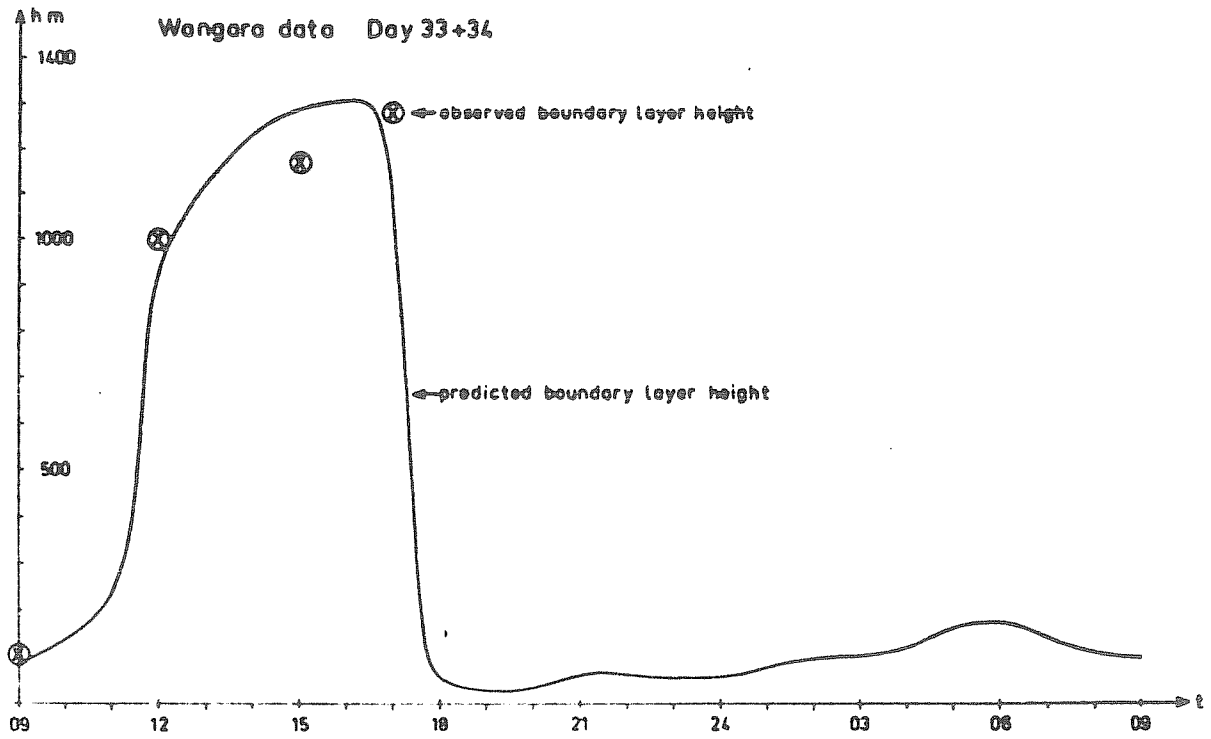

Fig.15 Predicted boundary layer height by Bodin´s model.Surface temperature variation prescribed.

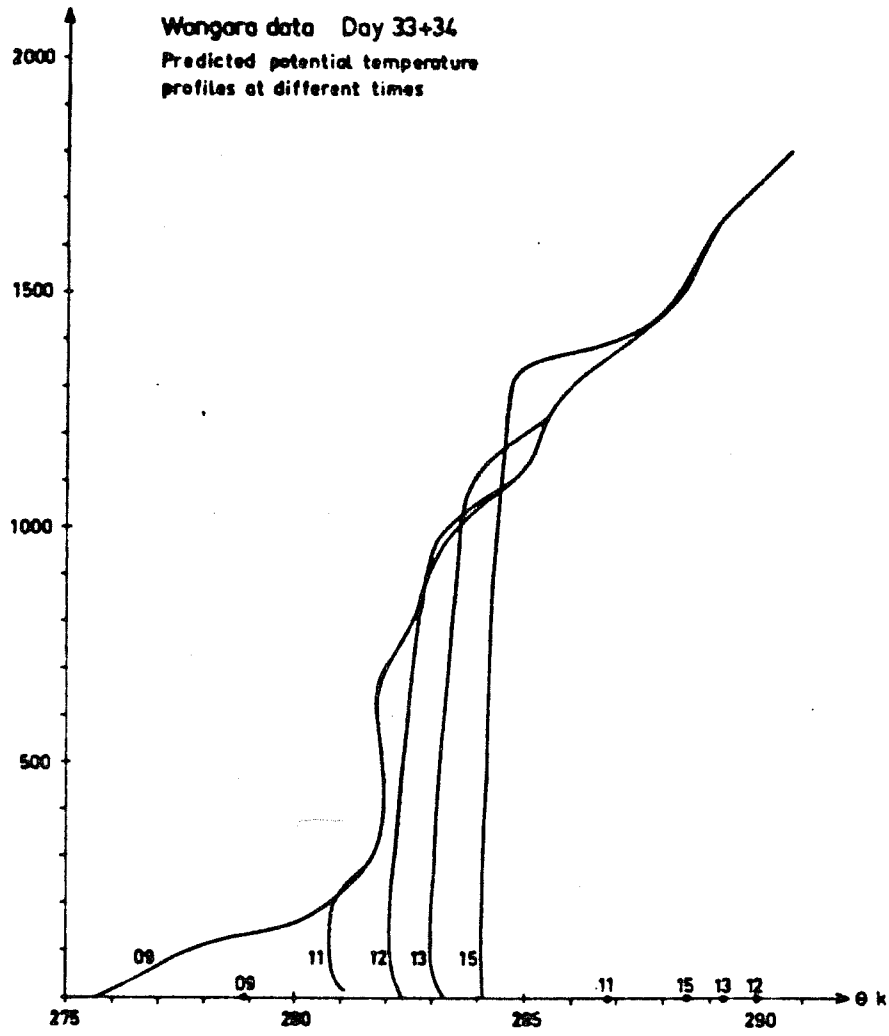

Fig.16 a)

Predicted potential temperature profiles. (for verification see fig.22)

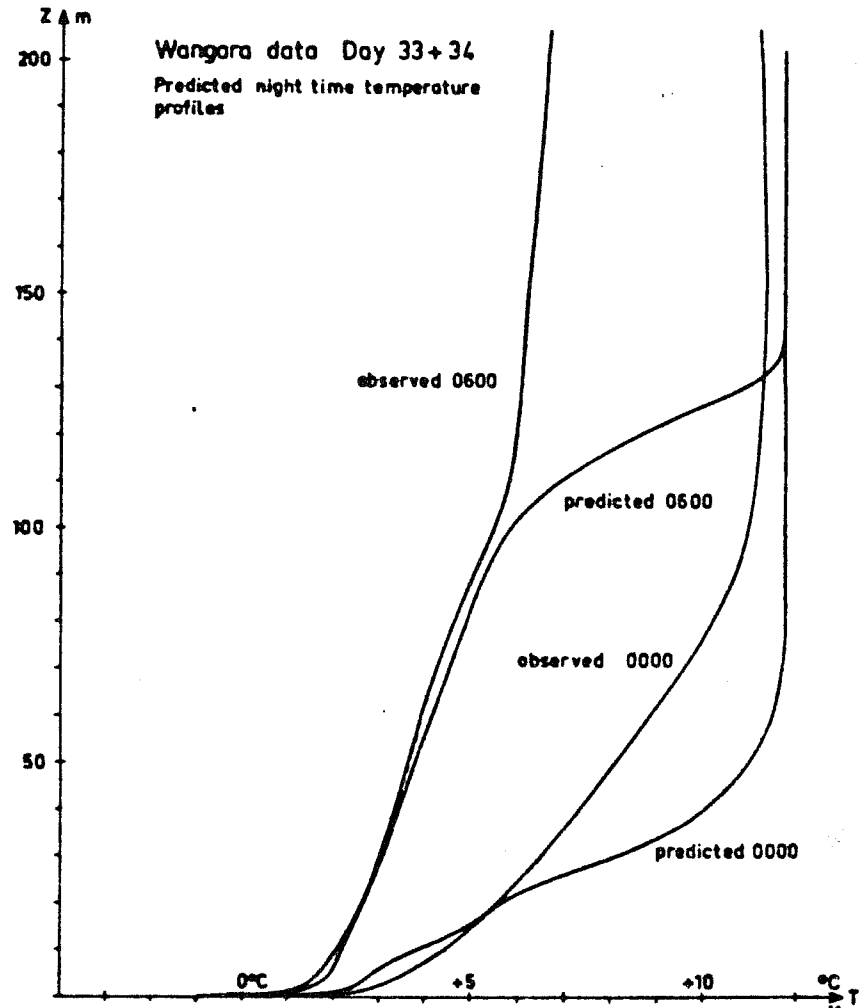

Fig.16 b)

Predicted and observed temperature profiles in the lowest 200 m of the nocturnal boundary layer. Bodin´s model.

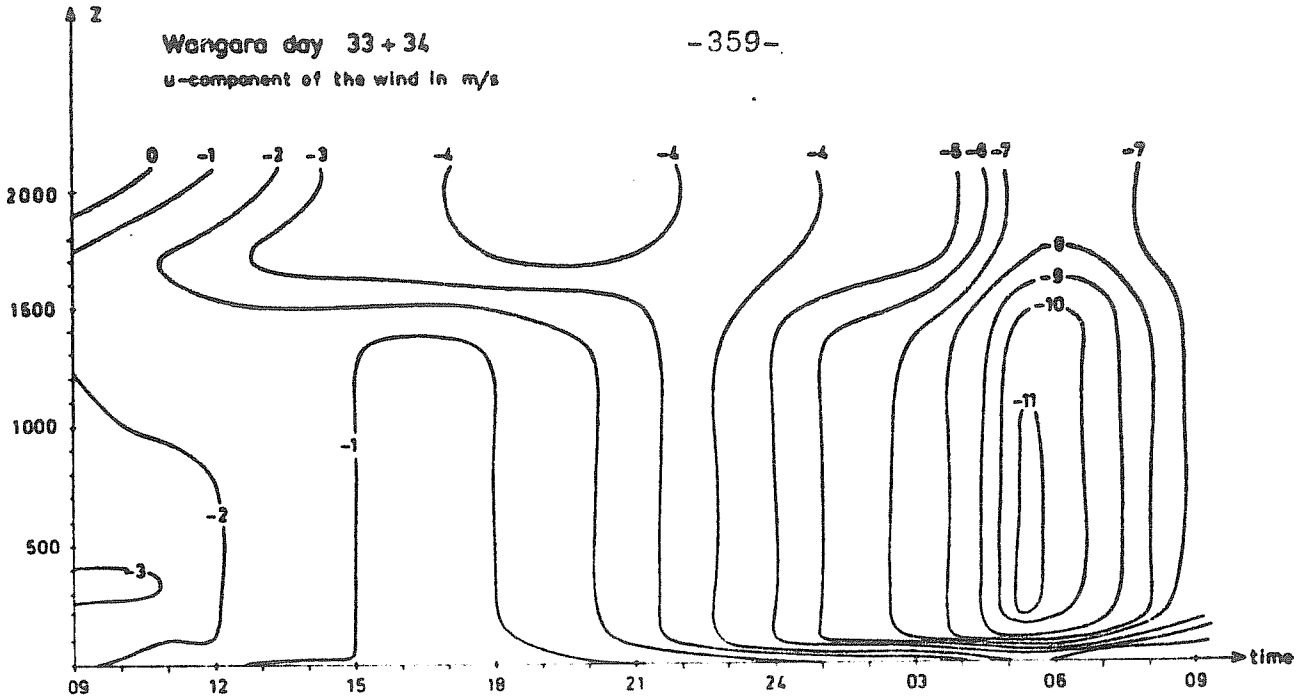

Fig.17 Predicted u-component of the wind(fig.11 for verification)

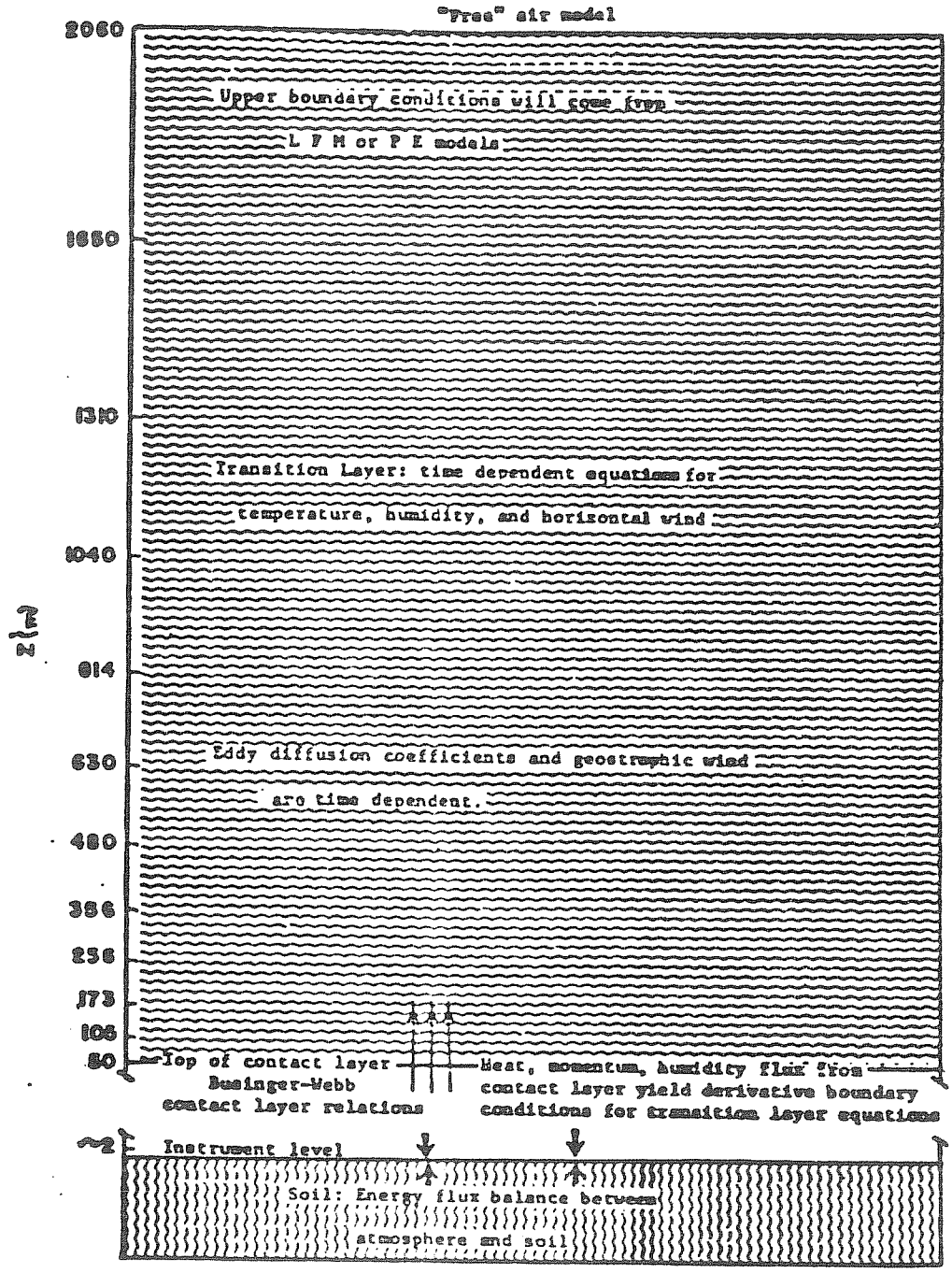

Fig.18

Vertical structure of Shaffer &Long´s model (1973)

1. 3-dimensional models

When saying there does not exist any operational ABL-model that is not entirely true. The U.S.AF. at AFGWC is running a 3-dimensional ABL-model operationally. That model was developed by Joe Gerrity (1967) in a pioneering attempt to predict low ceiling and cloudiness. That model was implemented in the U.S.AF. by Hadeen (1970). The model has also been run experimentally at NMC in order to evaluate its prognostic potential as reported by Poliger (1974).

However, even if the model has a positive skill in predicting for example type of precipitation its performance was not regarded as good enough to motivate its running operationally. In fact NMC finished the work with this model in favor of the 3-dimensional ABL-model being developed at TDL (Techniques development laboratory) by Wilson Shaffer & Paul Long, the latter presently with Du Pont in South Carolina.

It can be good to shortly review Gerrity's model since many features in his model have been used by others. One prime requirement on a 3-dimensional model is of course fast parameterization techniques of for example turbulence. All of the above discussed methods, fast as they are, are to slow to be able to be used in a 3-d model.

A natural way to go about is to eliminate the computations in the lowest 50 m by the introduction of a constant flux layer. For this end there exists the similarity theory of Monin-Obukov under conditions of stationarity and horizontal homogeneity. The basic part of the theory are the non-dimensional, universal functions ϕ_m, ϕ_n, ϕ_q of the argument z/L where L is the Monin-Obukov length. The surface layer relations can then be given by

$$\frac{kz}{u_*}\frac{\partial u}{\partial z} = \Phi_m(z/L), \tag{47}$$

$$\frac{kz}{\theta_*}\frac{\partial \theta}{\partial z} = \Phi_h(z/L), \tag{48}$$

$$\frac{kz}{q_*}\frac{\partial q}{\partial z} = \Phi_q(z/L) \tag{49}$$

$$L = \frac{u_*^2 \bar{\theta}}{k g \theta_*}$$ Monin-Obukov length.

$$u_* = \sqrt{\tau/\varrho} \qquad \theta_* = -\overline{w'\theta'}/u_* \qquad q_* = -\overline{w'q'}/u_*$$

The functions $\phi_i(z/L)$ have been determined in several observational programs. The ones mostly accepted nowadays are by Businger et. al. (1971) from the Kansas field program in 1968. (47)-(49) can be integrated through the surface layer and the fluxes depend on the boundary values at the surface and the top of the surface layer. They form a very fast and expedient way of calculating surface fluxes and they also give a corresponding eddy exchange coefficient for matching with the overlaying Ekman layer. Gerrity did not have these functions available in 1967 but used instead a semi-empirical formulation of K which also makes it possible to integrate the surface layer relations. On top of the surface layer he used an Ekman

layer for the wind, which was calculated diagnostically from a constant K being the same as at the top of the surface layer.
T and q are predicted by rate equations including non-adiabatic effects and turbulence. The forecast equations were descretized over an area containing 29 x 27 grid-points with a separation of 190.5 km, the griddistance of NMC´s LFM. Vertically the ABL is divided into 7 layers from the ground to 1600 m where the upper boundary condition on $\bar{V}g$,T and q are supplied from the LFM.
For finite differences Gerrity used Crank-Nicolson for the diffusion and vertical advection terms. For the horizontal advection terms upstream differences were used. This allowed a time step of Δt=15 minutes, longer than in any of the earlier models described. A weak point in Gerritys model was the very simple treatment of surface temperature and moisture at the lower boundary. Radiation was also simulated in a simple climatological way to keep down the time of integration.
Shaffer & Long´s work means a considerable extension of Gerrity´s model with a more refined and complete treatment of the physics in the ABL. But before we start the discussion about Shaffer & Long´s model it should be mentioned another model by Padro (1974) developed in Canada. His model is something half way between Gerrity and Shaffer & Long. He uses Businger´s surface relations and extends the corresponding K through the Ekman layer by means of a third order O´Brien interpolation polynomial. The winds in the Ekman layer are calculated diagnostically from steady state Ekman equations with a variable K(z). Δs is 127 km and Δt=30 minutes. Both Gerrity´s and Padro´s models utilize a terrain following height coordinate.

Shaffer & Long´s model (1973, 1975a, 1975b).

We will discuss this model at some length to study the way parameterization problems can be solved. The objective is to forecast mesoscale processes in the ABL to serve as guidance for local severe weather forecasting as well as regional air pollution dispersion prediction. Maybe it wouldn´t be necessary to repeat again the equation of motions used by Shaffer & Long. However, for the sake of completeness we write them down . In this case they are written in complex form in order to make use of the complex arithmetic on IBM 360/195.

$$\frac{\partial \tilde{T}}{\partial t} + \bar{V}\nabla\tilde{T} = \frac{\partial}{\partial z}\left(K_T \frac{\partial \tilde{T}}{\partial z}\right) + \tilde{Q} \qquad (50)$$

$$\frac{\partial \tilde{W}}{\partial t} + \bar{V}\nabla\tilde{W} = \frac{\partial}{\partial z}\left(K_m \frac{\partial \tilde{W}}{\partial z}\right) - i f(\tilde{W} - \tilde{G}) \qquad (51)$$

where $\tilde{T} = \vartheta + i\,q$, $\tilde{W} = u + i\,v$, $\tilde{G} = u_g + i\,v_g$

$K_T = K_q \neq K_m$, $\tilde{Q} = Q_h + i\,Q_q$

Fig. 18 shows schematically the vertical structure of the model. In the 50 m thick surface or Prandtl layer the relations (47)-(49) are used. The ϕ:s due to Businger et. al. have been used, i.e.

Unstable case:

$$\phi_q = \phi_T = 0.74\left(1 - 9\frac{z}{L}\right)^{-1/2} \quad (52)$$

$$\phi_m = \left(1 - 15\frac{z}{L}\right)^{-1/4} \quad (53)$$

Mildly stable: $$\phi_q = \phi_T = 0.74 + 4.7\frac{z}{L} \quad (54)$$

$$\phi_m = 1 + 4.7\frac{z}{L} \quad (55)$$

The advantage with the Businger relations is that they can easily be integrated. From the integrated form and the boundary condition u,v,θ and q u_*, θ_*, q_* and L can be calculated. With the fluxes given K_m and K_T in the surface layer may be computed from

$$K_T = k u_* z / \phi_T(z/L) \quad (56)$$

$$K_m = k u_* z / \phi_m(z/L) \quad (57)$$

with the aid of K_m, K_T, $\frac{\partial K_T}{\partial z}$ and $\frac{\partial K_m}{\partial z}$ an O'Brien (1970) cubic diffusion coefficient profile is used. It gives a maximum of K in the Ekman layer but is independent of local stability.

$$K = K_h + \left(\frac{z-H}{H-h}\right)^2\left(K_m - K_H + (z-h)\left[\left(\frac{\partial K}{\partial z}\right)_h + \frac{2(K_h - K_H)}{H-h}\right]\right) \quad (58)$$

where H is the top of the boundary (or the height where K takes on the specified value K_H, see below), h is the top of the surface layer.

Surface energy balance

The surface temperature depends on the sum of the fluxes at the surface. Shaffer & Long make use of a surface energy balance equation

$$\rho c_p u_* \theta_* + \rho L u_* q_* - F_{soil} - \epsilon_s \sigma T_{stc}^4 + R_{adnet} = 0 \quad (59)$$

where the two first terms are the surface heat flux and flux of latent energy respectively from the definition of θ_* and q_*. In order to close the system some assumption is needed for the surface value of q (z=0). In the model the so called Halstead parameter

$$H = E/E_p = \frac{q_h - q_{z=0}}{q_h - q_{z=\delta}} \text{(saturated)} \quad (60)$$

is set equal to a constant ≤ 1. From that q_* can easily be calculated. (compare eq. (46) in which H=f(w) is allowed to vary as a function of soil water content, w). In (59) the soil heat flux must also be given. It is usually calculated from a solution of soil temperature in the upper 1 m of the ground by means of eq. (35). However, initial profiles of T_s are hardly ever known

and the thermal diffusivity is a badly known quantity. In view of these difficulties Shaffer & Long have derived a very fast method for the calculation of surface soil heat fluxes. With the boundary conditions

T_s = constant $\qquad z \to \infty$

$T_s = T_{sfc} \qquad z = 0$

and a constant K_s the solution for surface temperature T_{sfc} can be written (see for example Carslaw & Jaeger (1959) for this standard solution of eq. (35)).

$$T_{sfc} = \frac{1}{\sqrt{\pi K_s t}} \int_0^\infty T_0(\xi) e^{-\xi^2/4K_s t} d\xi + \frac{1}{\lambda_s}\sqrt{\frac{K_s}{\pi}} \int_0^t \frac{F(t-u)}{\sqrt{u}} du \qquad (61)$$

where λ_s is the thermal conductivity, $T_o(z)$ the initial soil temperature profile. F(t) is the surface heat flux at time t. With a simple choice of $T_o(z)$, a linear profile for example, the first integral can easily be integrated. The second integral can be approximated by a sum of fluxes by using the trapezoidal method for example. Eq.(61) can then be solved for F(t) as a function of a weighted sum of the previous fluxes and the actual surface temperature. The next flux at time step $F(t+\Delta t)$ is a linear combination of the previous ones. Bodin (1974) has compared this method with a numerical, high resolution solution of eq. (35) with a varying surface temperature. Eq. (61) is more than sufficient for most applications!

Radiation

The model has a complete treatment of long wave and short wave radiation. This will not be discussed in detail here. However, the long wave radiation subroutine uses emissivity functions derived by Kuhn (1963), the same for the whole water vapor, spectral range. Kondratyev (1969) emissivities for CO_2 are used. The computation takes into account the presence of clouds in the ABL. That is true for the shortwave radiation computation as well. But also high and middle high clouds are allowed to absorb and reflect solar radiation. Fig. 19 shows this schematically.

Finite differences

Shaffer & Long also work with a terrain following coordinate z which is transformed to z' by

$$z' = A \ln\left(1 + \frac{z-h}{A}\right) + h \qquad (62)$$

where h is the top of the surface layer.
S & L then use 10 equidistant levels from the ground to 2000 m, the first one being at the top of the 50 m thick surface layer. Centered differences are used in the vertical and Laasonens scheme in time. For the horizontal advection terms so called "chapeau"-functions suggested by James Bradley, are used. In the x-direction they look

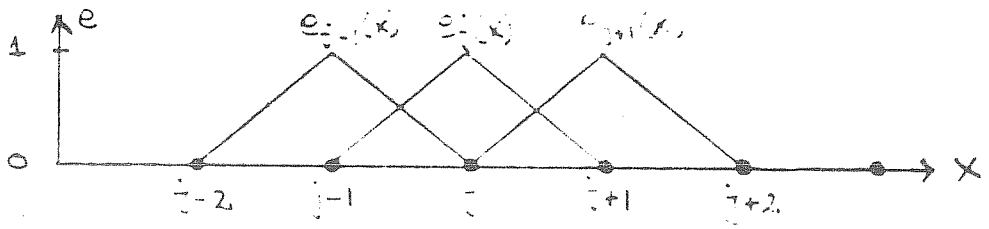

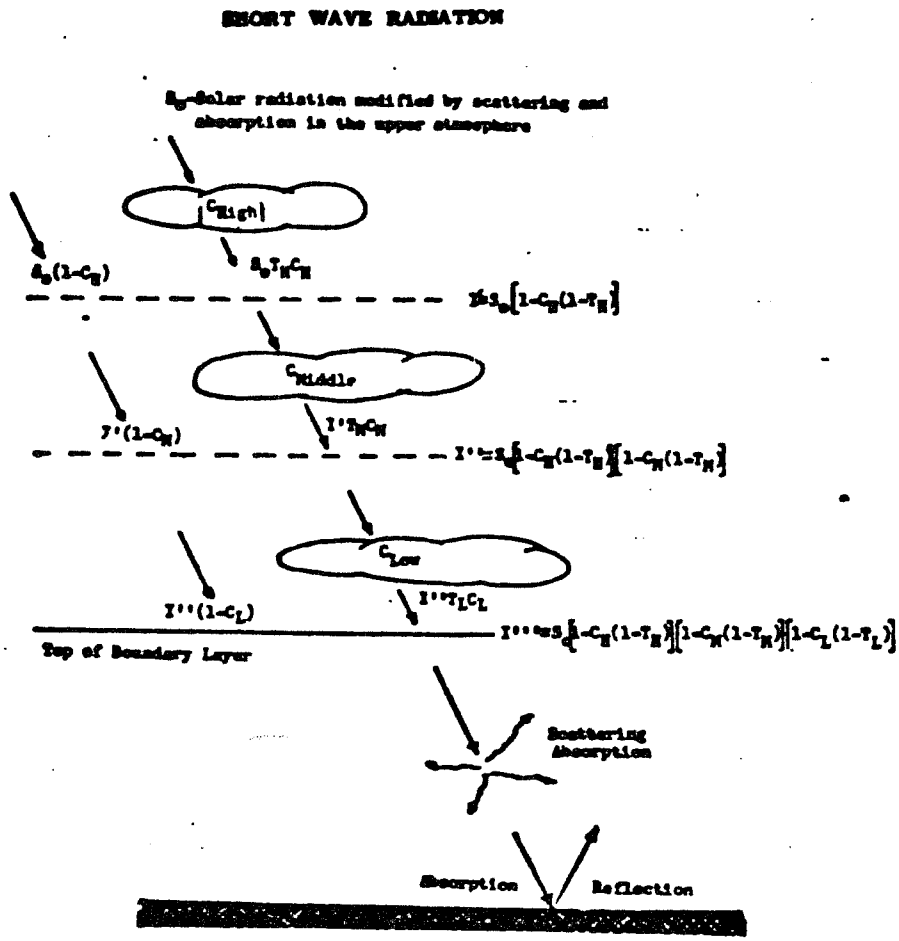

Fig.19 a) Treatment of solar radiation in Shaffer &Long´s model.

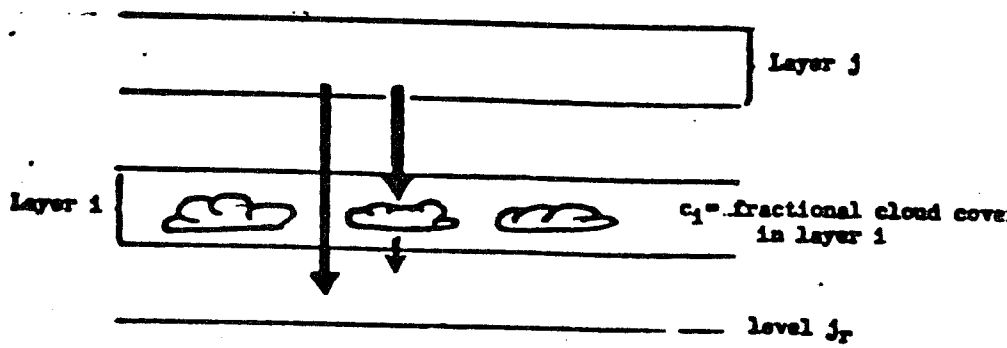

The amount of downward flux reaching j_r from layer j is

$$\sigma T_j^{\mu} \Delta E_j (1-c_j)$$

The amount of flux reaching j_r from layer i is

$$\sigma T_i^{\mu} \Delta E_i (1-c_i) + \sigma T_{\text{cloud base}}^{\mu} c_i (1-E(\text{cloud base}, j_r))$$

Fig.19 b) The same but for long wave radiation.

$e_j(x)$ is linearly increasing and decreasing if

$$x \in [x_{j-1}, x_{j+1}] \qquad (63)$$

$e_j(x) = 0$ if $x \notin [x_{j-1}, x_{j+1}]$

For example if (63) is introduced in the advection equation

$$\frac{\partial Q}{\partial t} + C\frac{\partial Q}{\partial x} = 0$$

by means of $Q(x,t) = \sum_{j=1}^{N} \alpha_j(t)\, e_j(x)$

and integrated over the domain we get

$$\frac{1}{6}\frac{\partial}{\partial t}(\alpha_{j-1} + 4\alpha_j + \alpha_{j+1}) + \frac{C}{2\Delta x}(\alpha_{j+1} - \alpha_{j-1}) = 0 \qquad (64)$$

This is a Galerkin approximation since

$$[e_j(x), R(x)] = 0$$

where R is the error of the finite difference approximation.

Eq. (64) can then be solved in different ways, for example by Laasonen's method as in this case. An analysis of this scheme shows that phase and group velocity are very well handled down to $3\Delta x$. In the 3-dimensional case a splitting technique is used.

Simulations

Shaffer & Long have done one-dimensional simulations of the Wangara data (Day 39,32) and the O'Neill data. (5th period) and also the sensitivity tests shown above. Furthermore Tsan Yu (1975) has tested the model with 13 different K-formulations with different stability dependence and one case with the turbulent energy equation above the surface layer. Fig. 20 shows an example of predicted temperature and wind for Day 39 of the Wangara data.

3d-version

Plans are to run the model on a 35 x 30 horizontal grid with 8 levels in the vertical. That would mean a $\Delta x = \Delta y = 80$ km which allows a time step of $\Delta t = \frac{1}{2}$ h. Jim Kemper has been working on the initialization and analysis package for the model. The region covered and the details of the topography are shown in fig. 21. The initialization problem has turned to be more difficult than expected. The continuity equation is not carried as a prognostic equation. Pressure is calculated diagnostically by means of the hydrostatic balance from the upper boundary condition from the LFM. The model doesn't allow gravity wave adjustment as a means for adjusting to "geostrophic" balance. This means that most of the energy go into local inertial-diffusive oscillations discussed above. It seems that some sort of variational technique á la Sasaki must be utilized in analysing the wind field with the equations of motion as a weak constraint. However, this is still an unsolved problem.

Pielke's and Tapp & White's models

These models are actually not intended to be operational models, at least not in the nearest future. Both are

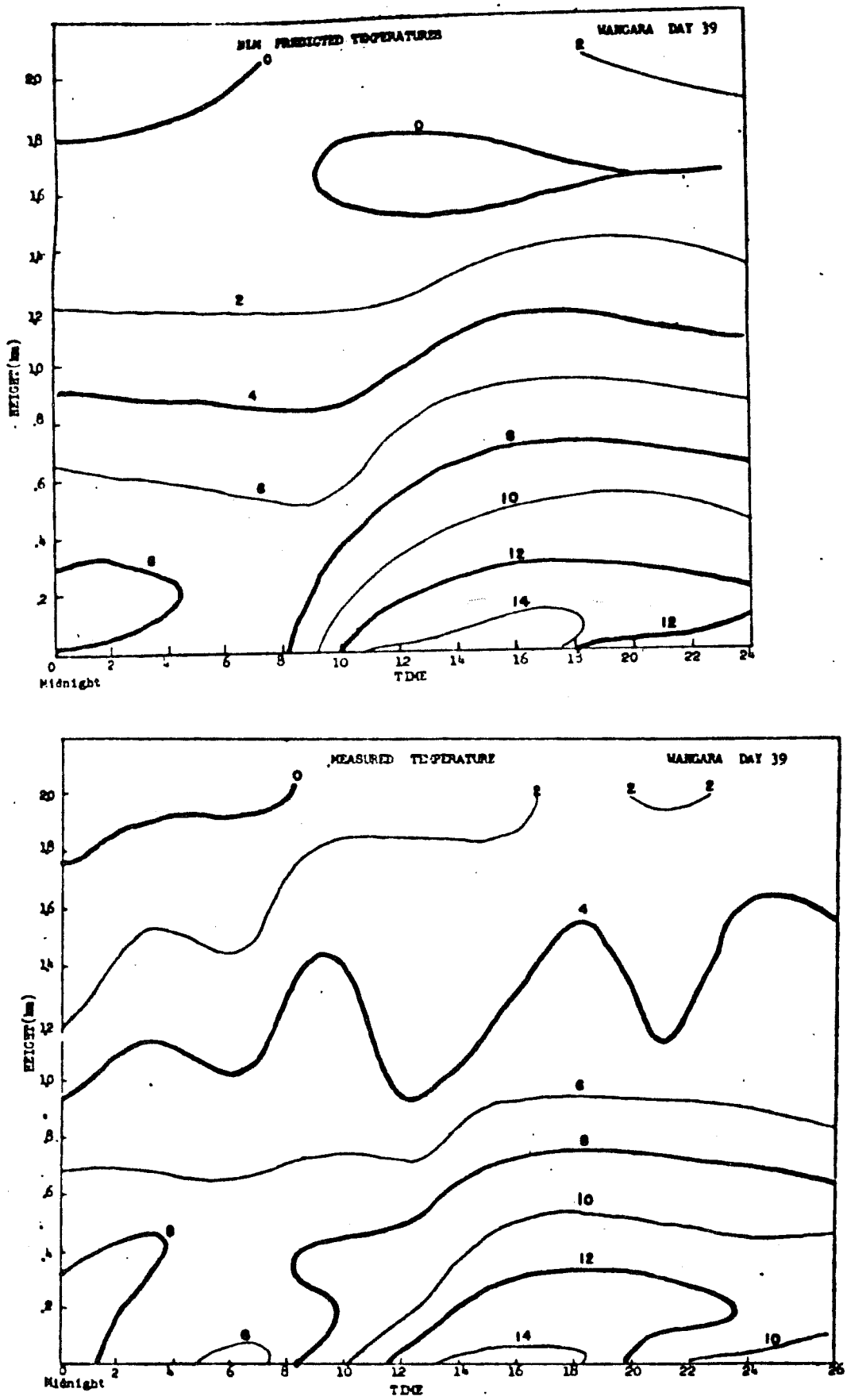

Fig.20 a) Predicted and observed time-height cross section for temperature for Day 39 of the Wangara data.Shaffer&Long´s one-dimensional model

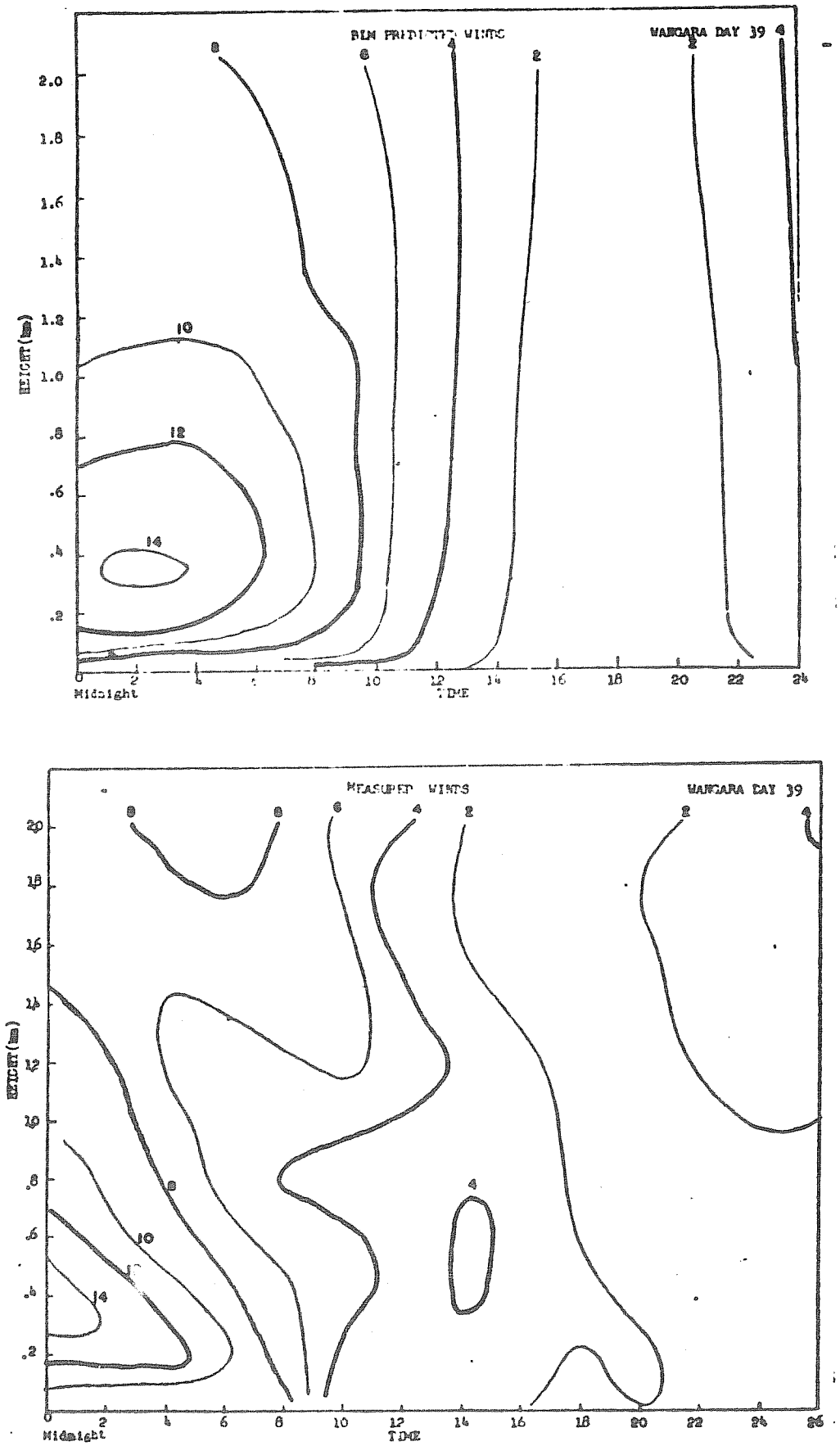

Fig.20 b) The same but for wind speed.

models intended to be used in sea-breeze simulations. There are, however, some interesting points in their models and for the sake of completeness they should be mentioned.

Pielkes model

The latest development of Pielkes model has been reported on in Pielke and Mahrer (1975). The basic structure of the model is essentially the same as Shaffer & Long's model. In the paper from 1975 they have made one important improvement. In the O'Brien K-profile K is set to zero at some upper level, for example 2000 m, the top of model. This formulation is uncapable of describing the observed and theoretically modelled growth of the undisturbed convective boundary layer. In P & M they introduce a rate equation for the height of the ABL suggested by Deardorff (1974), neglecting the influences of clouds.

$$\frac{\partial h}{\partial t} = -\nabla \tau h + w_h + \frac{1.3(w_*^3 + 1.1u_*^3 - 2.3u_*^2 fh)}{\frac{h^2}{h_c}\frac{\partial \theta^*}{\partial z} + 7.0w_*^2 + 7.2u_*^2} \qquad (65)$$

where $\frac{\partial \theta^*}{\partial z}$ is the lapse rate above the capping inversion

$$w_* = (-2u_*\theta_* h/\theta_v)^{1/3}$$

W_h = vertical velocity at the inversion level.

If we now instead apply the top of the O'Brien profile at z=h this simple model is significantly improved as shown in the simulation by P & M of the day 33 Wangara data. Fig. 22 shows the predicted θ-profiles for 12,15,18 o'clock with a one-dimensional version of the model run with 31 levels in the vertical. As can be seen a simple turbulence parameterization as this is then fully capable of depicting the evolution of the unstable boundary layer. The same procedure with a rate equation has now also been adopted by Shaffer and collaborators. One must keep in mind that this method is considerably faster than any other method. The same equation can be extended to the nocturnal ABL. However, the nocturnal ABL is much more difficult to treat than the unstable ABL because of the presence of patchy, breaking gravity wave induced turbulence.

Tapp & White's model

This is described in a recent paper, Tapp & White (1976). The main difference from the other models is that T & W's model is non-hydrostatic and allow sound waves as solutions of the equations. T & W discuss at some length the implications of the presence of the soundwaves and the finite difference scheme developed for the model. In order to allow a reasonably long time step they treat the equations semi-implicity. But even by doing so they have to use a timestep as short as 60 seconds, which is hardly long enough in an operational context where additional physical parameterizations are needed. But as a 3-dimensional simulation model it has certain advantages. They have also compared the performance of the model with Pielke's model, Pielke (1973). The differences between the hydrostatic and non-hydrostatic model seem to be small when the models are run with similar resolution.

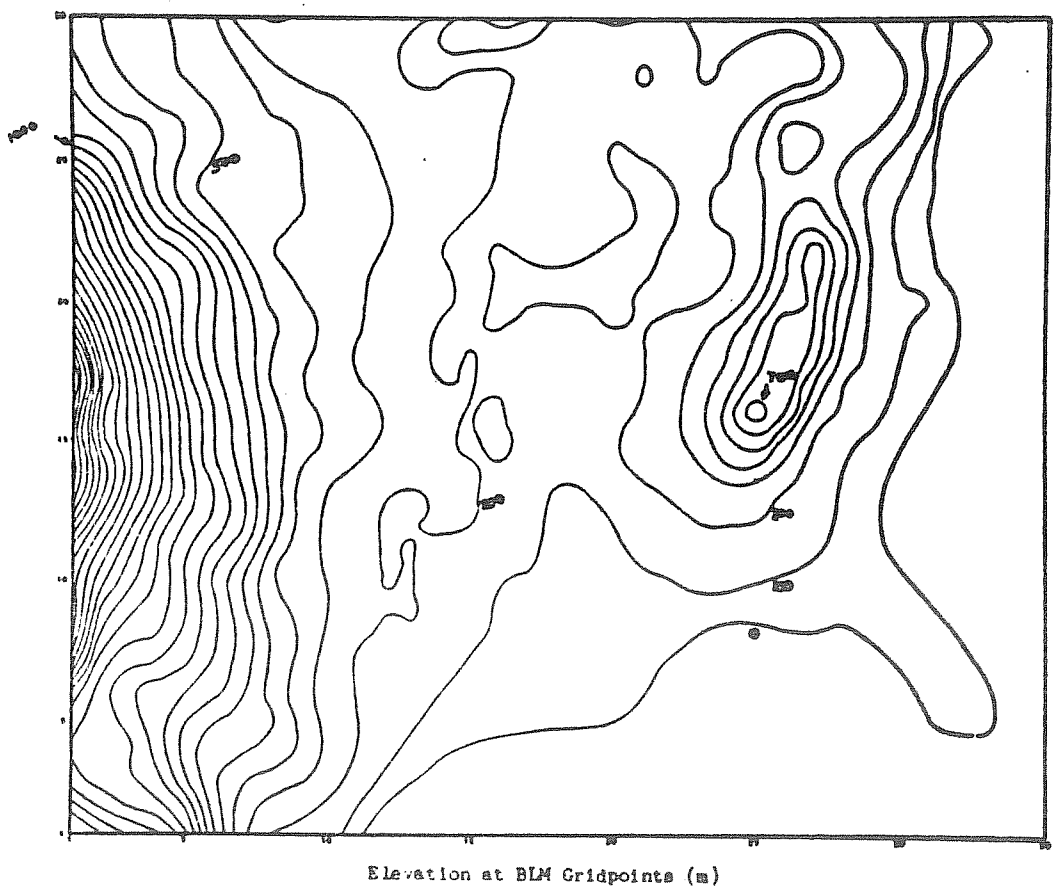

Fig.21 Topography in the region of the U.S.A. used in Shaffer&Long's 3-dimensional model.

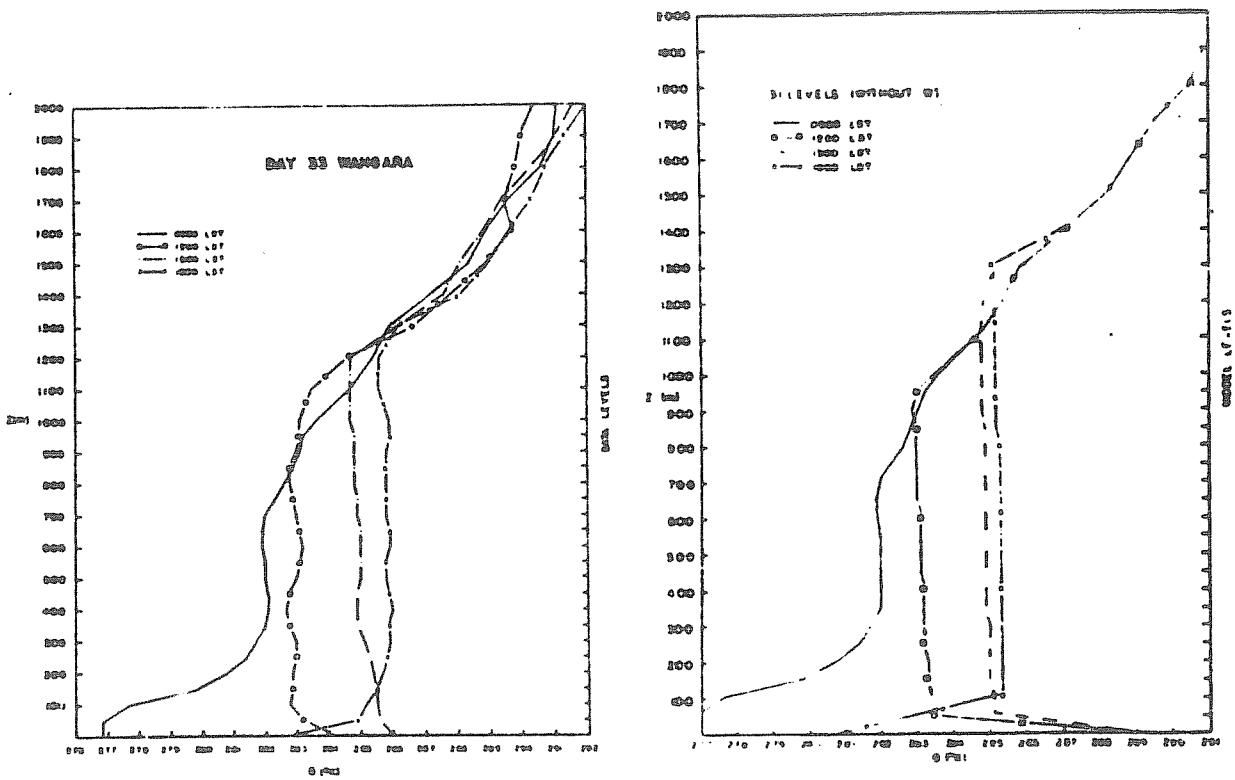

Observed Predicted

Fig.22 Observed and predicted virtual potential temperature profiles.(from Pielke&Mahrer,1975)

5. Conclusions and remaining problems

We can clearly see that we are at the verge of a breakthrough in numerical ABL-models. In the present review I have showed you examples of some models people are working with today. The list is not complete, however. Other interesting modelling attempts are carried out by for example Kaplan & Paine (1974) and Geleyn (1975) and others. But I have wanted to concentrate on some characteristic problems of "operational" models and how they might be solved. We have seen that in a one-dimensional model one can afford much more realistic parameterizations of basic physical processes as turbulence in the ABL at the expense of horizontal variation of topography, roughness and heat and moisture properties of the underlying surface. In the 3-dimensional models on the other hand one has to sacrifice a more refined turbulence description in favor of a simplified one. We have seen that there exist fast and fairly accurate methods for this end. One drawback is that most of these methods, Monin-Obukhov similarity, have been developed under rather strict premises of stationarity and horizontal homogeneity. Evidence is available showing that similarity breaks down in a number of situations in the "real life" boundary layer. It is therefore clear that a continued research effort by theoreticians and "higher order scheme" modelers is needed to provide improved methods for turbulence parameterizations, including physical processes in the real ABL and especially under stable stratification.

The other, virtually untouched, problem is about data requirements, analysis and initialization of operational boundary layer models. We have already mentioned the problems with the false inertial-diffusive oscillations. But we have very little experience of what kind of data we need for running an ABL-model with at least some skill. Very practical problems concern the collecting of surface characteristics data. We need z_o, thermal diffusivity and thermal conductivity as well as moisture content of the ground over fairly large areas. But we do not need them as point values but as effective areal values over grid squares where we can have a mixture of different vegetations and soil types. The best thing to do is probably to prepare magnetic tapes with land-use data.

References:

Barr & Kreitzberg, 1975: Horizontal variability and boundary layer modelling, Boundary Layer Meteorology. No. 2 (8).

Bodin, S., 1974: Development of an unsteady atmospheric boundary layer model. SMHI Reports, Meteorology and Climatology, No. 2.

Bodin, S., 1976: An unsteady one-dimensional atmospheric boundary layer model. Paper to be presented at WMO Symposium on Interpretation of broad-scale NWP, Warsaw, 11-16 October 1976.

Brown, R. & Roach, W.T., 1976: The physics of radiation fog: II-a numerical study. QJRMS, Vol. 102, p. 335.

Businger, J. A., et. al., 1971: Flux-profile relationships in the atmospheric surface layer. JAS, 28 (3), 181.

Ching, J.K.S., Businger, J.A., 1968: The response of the planetary boundary layer to time varying pressure gradient force. JAS, 25, p. 1021.

Clarke, R.H.: Attempts to simulate the diurnal course of meteorological variables in the boundary layer. Unpublished paper.

Clarke, R.H., et. al., 1971: The Wangara experiment: Boundary layer data. CSIRO, Division of Meteorological Physics Techn. Paper, No. 19.

Deardorff, J.W., 1973: The use of subgrid transport equations in a three-dimensional model of atmospheric turbulence. Paper presented at the Applied Mechanics and Fluid Engineering Conference, Atlanta, Ga, June 1973.

Deardorff, J.W., 1974: Three-dimensional numerical study of the height and mean structure of a heated planetary boundary layer. Boundary Layer Meteorology, 7, p. 81-106.

Geleyn, J.F., 1975: Un modèle unidimensionelle et son application a l'étude du cycle diurne. La Météorologie, No. 2, 1975.

Gerrity, J.P., 1967: A physical-numerical model for the prediction of synoptic-scale cloudiness. Monthly Weather Review, 95 (5).

Gutman, L.N., 1969: Introduction to the non-linear theory of mesoscale meteorological processes. Leningrad 1969. English translation, Israel Program for Scientific translations, Jerusalem 1972.

Hadeen, K.D., 1970: AFGWC Boundary layer model. AFGWC Tech. Memo 70-5, Air Force Global Weather Central, Offut AFB, Neb., U.S.A.

Kaplan, M.L. & Paine, 1974: The quasi-hydrostatic modes of gravitational adjustment and their implications for the operational numerical forecasting of severe local storms. Workshop on subsynoptic extra tropical weather systems. NCAR, Boulder, U.S.A.

Kondratyev, K. Ya., 1969: Radiation in the atmosphere. International Geophysics series, 12, Academic Press, New York.

Kuhn, P.M., 1963: Radiometersonde observations of infrared flux emissivity of water vapor. JAM, 2, p. 368.

Long, P.E., Shaffer, W.A., 1975: Some physical and numerical aspects of boundary layer modelling. NOAA Techn. Memorandum NWS TDL-56.

Long. P.E., 1975: Dissipation, dispersion and difference schemes, NOAA Techn. Memorandum NWS TDL-55.

Mellor, G.L., Yamada, T., 1974: A hierarchy of turbulence closure models for planetary boundary layers. JAS, 31, October, p. 1791.

O'Brien, J.J., 1970: A note on the vertical structure of the eddy exchange coefficient in the planetary boundary layer. JAS, 27, p. 1213.

Padro, J., 1974: Forecasting in the planetary boundary layer. Preliminary report, Atmospheric Environment, Canada.

Pielke, R.A., 1973: A three dimensional model of the sea breezes over south Florida, NOAA Tech. Mem. ERL WMPO-2.

Pielke, R.A. & Mahrer, Y., 1975: Representation of the heated Planetary Boundary layer in mesoscale models with coarse vertical resolution. JAS, 32, Dec. 1975.

Poliger, P., 1974: An evaluation of the NMC:s experimental boundary layer model. NOAA Techn. Memorandum NWS NMC-55.

Shaffer, W.A., Long, P.E., 1973: A predictive boundary layer model. Presented at the symposium on the Atmospheric Boundary Layer in Mainz, Germany, October 1973.

Speranskiy, Lykosov and Gutman, 1975: The turbulent Planetary Boundary layer above a curvilinear underlying surface in the presence of horizontal heat advection. Izv. Atmospheric and Oceanic Physics, Vol. 11, No. 5. English translation.

Tapp, M.C. & White, P.W., 1976: A non-hydrostatic mesoscale model. QJRMS, Vol. 102, No. 432. p. 277.

Tsan Yu, 1975: Numerical experiments using various K-theories in a planetary boundary layer model. Paper presented at AMS First Conference on Regional and mesoscale modelling, analysis and prediction, Las Vegas, U.S.A.

Yamada, T., Mellor, G., 1975: A simulation of the Wangara atmospheric boundary layer data. Report from the 1rst AMS Conference on Regional and Mesoscale Modelling, Analysis and Prediction, Las Vegas, U.S.A.

Zdunkowski, W.G., Barr, A.E., 1972: A radiative - conductive model for the prediction of radiation fog. Boundary Layer Meteorology, 3, p. 152.